Metabolic Engineering 49 (2018) 69–83

Contents lists available at ScienceDirect

Metabolic Engineering

journal homepage: www.elsevier.com/locate/meteng

Multi-omic elucidation of aromatic catabolism in adaptively evolved *Rhodococcus opacus*

William R. Henson[a,1], Tayte Campbell[b,1], Drew M. DeLorenzo[a,1], Yu Gao[a], Bertram Berla[b,c], Soo Ji Kim[a], Marcus Foston[a], Tae Seok Moon[a,*], Gautam Dantas[b,c,d,e,**]

[a] Department of Energy, Environmental and Chemical Engineering, Washington University in St. Louis, St. Louis, MO 63130, USA
[b] The Edison Family Center for Genome Sciences and Systems Biology, Washington University in St. Louis School of Medicine, St. Louis, MO 63110, USA
[c] Department of Pathology and Immunology, Washington University in St. Louis School of Medicine, St. Louis, MO 63108, USA
[d] Department of Biomedical Engineering, Washington University in St. Louis, St Louis, MO 63130, USA
[e] Department of Molecular Microbiology, Washington University in St. Louis School of Medicine, St. Louis, MO 63108, USA

ARTICLE INFO

Keywords:
Adaptation
Aromatic tolerance
Funneling pathway
Lignin
Redox metabolism

ABSTRACT

Lignin utilization has been identified as a key factor in biorefinery profitability. However, lignin depolymerization generates heterogeneous aromatic mixtures that inhibit microbial growth and the conversion of lignocellulose to biochemicals. *Rhodococcus opacus* is a promising aromatic-catabolizing, oleaginous bacterium, but mechanisms for its aromatic tolerance and utilization remain undercharacterized. To better understand these mechanisms, we adaptively evolved *R. opacus* for improved utilization of 32 combinations of diverse aromatic compounds. Evolved *R. opacus* mutants showed up to 1900% growth improvement in the utilization of phenol, guaiacol, 4-hydroxybenzoate, vanillate, and benzoate compared to the wild-type strain. Whole genome sequencing revealed several redox-related genes with mutations shared across multiple adapted mutants. PVHG6, the mutant with the most improved growth on a mixture of multiple aromatic compounds, showed 56% lower superoxide dismutase activity than the wild-type strain, suggesting that redox reactions are important for aromatic tolerance and utilization. Comparative transcriptomics revealed by-product detoxification pathways and five aromatic funneling pathways that were upregulated in response to specific aromatic compounds. Gene knockout experiments confirmed the two degradation routes of the β-ketoadipate pathway for five aromatic compounds. These results provide an improved understanding of aromatic bioconversion and facilitate development of *R. opacus* as a biorefinery host.

1. Introduction

Lignocellulosic biomass is a potential source of renewable bio-based fuels and chemicals. A large fraction of lignocellulose (~ 70–85%) is cellulose and hemicellulose, which can be depolymerized into monomeric sugars, such as glucose and xylose (Sun and Cheng, 2002; Wheeldon et al., 2017). The remaining 15–30% of lignocellulose is lignin, a highly cross-linked, heterogeneous, and recalcitrant aromatic polymer (Pandey and Kim, 2011). Microbial conversion of lignocellulose holds promise as a new way to produce a variety of novel products and petrochemical replacements (e.g., drop-in fuels) (Bhat et al., 2015; Hahn-Hagerdal et al., 2006; Jones et al., 2016; Lee et al., 2016; Pereira et al., 2016; Qiao et al., 2017; Xu et al., 2016; Yang et al., 2018; Zhou et al., 2016a, 2016b). Current biomass pretreatment approaches, which aim to increase sugar extractability from lignocellulose, also release aromatics from lignin that negatively affect microbial product titers, yields, and productivities (Ibraheem and Ndimba, 2013; Pienkos and Zhang, 2009). Current processes separate the carbohydrate fraction from the lignin fraction, and the separated lignin is either discarded or burned for process heat or on-site electricity generation (Ragauskas et al., 2014). However, removal of lignin-derived inhibitors from sugar streams is still challenging and costly, and techno-economic analyses have identified the co-utilization of lignin as an important factor in biorefinery profitability (Balan et al., 2013; Valdivia et al., 2016). Therefore, efforts are underway to develop microbial strains that can tolerate and convert inhibitory, lignin-derived

* Corresponding author at: Department of Energy, Environmental and Chemical Engineering, Washington University in St. Louis, St. Louis, MO 63130, USA.
** Corresponding author at: The Edison Family Center for Genome Sciences and Systems Biology, Washington University in St. Louis School of Medicine, St. Louis, MO 63110, USA.
E-mail addresses: tsmoon@wustl.edu (T.S. Moon), dantas@wustl.edu (G. Dantas).
[1] These authors contributed equally to this work.

https://doi.org/10.1016/j.ymben.2018.06.009
Received 1 March 2018; Received in revised form 29 May 2018; Accepted 14 June 2018
Available online 27 July 2018

compounds into value-added products (Blazeck et al., 2014; Bugg and Rahmanpour, 2015; Dunlop, 2011; Fischer et al., 2008; Henske et al., 2017; Jin and Cate, 2017; Keating et al., 2014; Le et al., 2017; Pham et al., 2017; Vardon et al., 2015).

Rhodococcus opacus PD630 (hereafter *R. opacus*) is a promising bacterial strain for producing valuable products from lignocellulose. *R. opacus* is a gram-positive soil bacterium that has been shown to have an inherently high tolerance to aromatic compounds (Alvarez et al., 1996; Tsitko et al., 1999). Additionally, it accumulates high levels (up to ~ 78% as cell dry weight) of the biofuel precursor triacylglycerol (TAG) and demonstrates a moderately high growth rate (Alvarez et al., 1996; Kurosawa et al., 2010). *R. opacus* can natively consume, or has been engineered to consume, hexose and pentose sugars present in lignocellulosic feedstocks (Kurosawa et al., 2010, 2013). *R. opacus* can also consume aromatic compounds found in depolymerized lignin, such as phenol, 4-hydroxybenzoate, and vanillate (Kosa and Ragauskas, 2012; Xie et al., 2017; Yoneda et al., 2016), making it uniquely qualified to utilize all three primary depolymerized components of lignocellulose.

The co-consumption of mixtures of lignin-derived aromatic monomers is an underexplored area of study that is important for microbial lignin conversion strategies. The inherent heterogeneity of lignin is a major barrier to lignin valorization, and economical strategies require rapid conversion of complex aromatic mixtures to products (Linger et al., 2014; Rodriguez et al., 2017; Shuai et al., 2016; Van den Bosch et al., 2017). Microbial degradation of diverse aromatic compounds is typically accomplished by biological funneling, where compounds are converted into common metabolites (e.g., catechol and protocatechuate), prior to their catabolism via a central aromatic degradation pathway, such as the β-ketoadipate pathway (Harwood and Parales, 1996; Linger et al., 2014). However, interactions between similarly structured compounds and different aromatic degradation pathways are not well understood in bacteria. Additionally, cross tolerance between lignin-derived aromatics has not been studied in *R. opacus*, although it is thought that low concentrations of multiple inhibitory compounds can negatively affect bacterial growth more than high concentrations of a single inhibitory compound on its own (Kurosawa et al., 2015).

The underlying mechanisms for aromatic tolerance and utilization in *R. opacus*, and microbes in general, are not well understood due to the complexity of the phenotype, which limits the use of rational strain engineering. One methodology for improving aromatic tolerance is through adaptive evolution, where evolutionary selection pressure is applied to the organism through serial subcultures (Conrad et al., 2011; Lenski and Travisano, 1994). *R. opacus* has been demonstrated to be amenable to adaptation for improved growth in the presence of different inhibitors from lignocellulosic hydrolysates (e.g., furans, organic acids, and phenolics) (Kurosawa et al., 2015), but the mechanistic basis for these improvements are unknown. Our previous work showed that *R. opacus* could be adapted for improved growth and lipid production on the lignin model compound phenol as a sole carbon source (Yoneda et al., 2016), and we identified the upregulation of aromatic degradation pathways and transporters as potential mechanisms of improvement in the adapted strains. However, phenol is only one of many potential aromatic compounds from lignin (Rodriguez et al., 2017; Shuai et al., 2016; Van den Bosch et al., 2017), and additional research is required to understand *R. opacus*' ability to adapt to mixtures of lignin-derived model compounds.

In this work, *R. opacus* was adaptively evolved on 32 combinations of six lignin model compounds (without added sugars) to study the capacity to improve its aromatic tolerance and utilization (Fig. 1). Comparative genomic analysis of 35 improved adapted strains identified a high percentage of mutations in oxidation and reduction (redox) related genes, several of which were shared across multiple strains from different adaptation conditions. We demonstrated that the activity of one of these targeted enzymes, superoxide dismutase, was 56% lower in PVHG6 (a mutant adapted for improved growth on a mixture of multiple compounds) than the wild-type (WT) strain. This suggests that reactive oxygen species may be important for aromatic tolerance and utilization. To examine whether aromatics were consumed individually or concurrently, targeted metabolomics was performed, revealing that compounds were consumed in a distinct order and that the PVHG6 strain co-consumed lignin model compounds at faster rates than the WT strain. We performed RNA-Seq on PVHG6 and WT grown on individual lignin model compounds and their mixture (without added sugars) to elucidate genes and pathways related to aromatic catabolism.

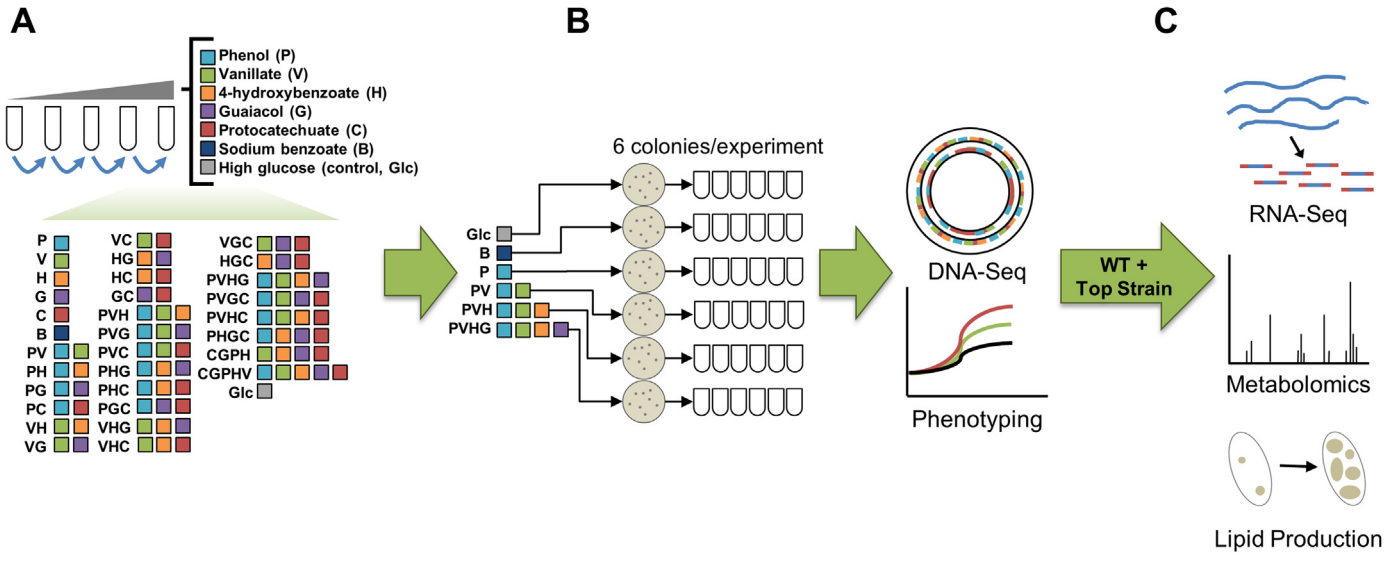

Fig. 1. Experimental approach. A. *R. opacus* PD630 was serially passaged on lignin model compounds and high glucose (33 conditions). Six adapted cultures were selected for further characterization: four using phenol and up to three other lignin model compounds, one using sodium benzoate, and one using high glucose as carbon sources. B. Six colonies from the selected adapted cultures were phenotyped in adaptation growth conditions to determine improvement compared to the WT strain. Strains with improved growth (OD_{600}) compared to the WT strain were characterized by whole genome sequencing and growth assays using mixtures of lignin model compounds. C. The best-performing adapted strain (PVHG6) and the WT strain were further characterized using RNA-Seq and targeted metabolomic analyses to identify mechanisms for improved lignin model compound tolerance and utilization. Lipid titers were measured to characterize the adapted strain's capacity to convert lignin model compounds into lipids.

Transcriptomic analyses identified five distinct funneling pathways and two by-product detoxification pathways, each of which is activated by specific aromatic compounds, as well as a number of upregulated transporters. Additionally, by gene knockout experiments, we confirmed the degradation routes of five aromatic compounds and the importance of upregulated transporters for growth on aromatic compounds. Lastly, to demonstrate that our improved aromatic tolerance and utilization phenotypes are compatible with production of valuable products from lignin, we measured lipid production and observed a 225% increase in lipid titer with the PVHG6 strain relative to the WT strain when grown on 2.5 g/L total aromatics as a sole carbon source. Together, these results advance our understanding of aromatic mixture tolerance and catabolism, which is a critical first step toward future fuel and chemical production from lignocellulose, and establish *R. opacus* as a promising bioproduction strain.

2. Materials and methods

2.1. Chemicals and strains

Chemicals were purchased from Sigma Aldrich (St. Louis, MO) unless otherwise indicated, and *Rhodococcus opacus* PD630 (DSMZ 44193) was used as the ancestral strain (WT) for comparison to all mutated strains. For all growth experiments (unless otherwise indicated), cells were grown at 30 °C and 250 rpm in one of two defined minimal salts media (A or B; medium composition as previously described (DeLorenzo et al., 2017)). Culture media were filter-sterilized using a 0.22 μm filter, and pH was adjusted to 7.0 using 6 M HCl or 2 M NaOH. Carbon and nitrogen sources were added as sterile-filtered stock solutions. *R. opacus* strains were maintained on tryptic soy broth (TSB) plates supplemented with 1.5% agar.

2.2. Adaptive evolution and growth assays of adapted strains

R. opacus was serially passaged on combinations of protocatechuate (PCA), guaiacol (GUA), phenol (PHE), 4-hydroxybenzoate (HBA), and vanillate (VAN) as carbon sources, and it was also passaged on each compound individually (Fig. 1). *R. opacus* was also adapted on sodium benzoate (BEN) and high concentrations of glucose individually as sole carbon sources. Minimal medium A was used for adaptation experiments. To start adaptation experiments, a single colony of the ancestral strain from a TSB agar plate was grown at 30 °C in 2 mL of minimal medium A supplemented with 0.3 g/L PHE for 24–48 h, followed by a subculture using an initial OD_{600} of 0.05 in 10 mL of the same media for 24 h. Next, cells were centrifuged at 3000 *g* for 10 min and resuspended in minimal medium A without carbon or nitrogen sources, and adaptation experiments were performed at a 10 mL culture volume in a 50 mL glass culture tube with the corresponding carbon source(s) (Table S1) and 1 g/L ammonium sulfate as the nitrogen source. For passaging, cultures were started at an initial cell density (OD_{600}) of 0.03. After ~ 30 passages, the initial cell density was increased to 0.05 for all adaptation experiments. Cells were passaged after reaching mid-exponential phase (OD_{600} > 0.3), and cells from each adaptation experiment at each passage were stored at − 80 °C in 15% glycerol. At each passage, the total aromatic concentration was increased by 1–5% until we did not observe growth after three days. If cells did not grow after three days, the culture was restarted from the previous −80 °C frozen stock, and the overall aromatic concentration was decreased until cell growth could be recovered. Once growth was recovered, the concentration was held constant for multiple passages before increasing concentrations in following passages. Adaptation experiments were stopped when we observed no growth after restarting adaptations from frozen stocks or adaptations reached > 100 passages. See Table S1 for details on adaptation experiments.

To isolate colonies, adapted cultures were streaked on minimal medium plates supplemented with 1.5% agar, 1 g/L ammonium sulfate, and respective carbon sources from the adaptation experiment (concentrations as indicated in Table S14). Six colonies were picked and grown at 30 °C in a 5 mL culture volume in a 50 mL glass tube with minimal medium A supplemented with 5 g/L glucose and 1 g/L ammonium sulfate for 36 h before storage at − 80 °C in 15% glycerol. To compare the phenotype of the isolated colonies to that of the WT strain using their adaptation carbon sources (Fig. 2), frozen stocks of each isolated strain were streaked on TSB plates and a single colony was grown in 2 mL of minimal medium A supplemented with lignin model compounds from their adaptation condition (concentrations as indicated in Table S14) for 24–48 h, and then subcultured using an initial OD_{600} of 0.05 in 10 mL of lignin model compounds from their adaptation condition (concentrations as indicated in Table S15) for 24 h. Next, cells were centrifuged at 3000 *g* for 10 min and resuspended in minimal medium A without carbon or nitrogen sources, and experiments were performed at 30 °C with a 10 mL culture volume in a 50 mL glass culture tube with adaptation carbon source(s) (concentrations as indicated in Fig. 2) and 1 g/L ammonium sulfate as the nitrogen source. Growth was monitored using absorbance at 600 nm (Abs_{600}). Absorbance measurements were made with black 96 well plates (Greiner Bio One) using a TECAN Infinite M200 Pro plate reader. OD_{600} values were obtained by converting the Abs_{600} of 200 μL of cell culture to OD_{600} using an experimentally determined correlation curve (OD_{600} = 1.975 * [Abs_{600} − 0.04], R^2 = 1.00). Specific growth rates were calculated by fitting at least four converted OD_{600} values in the log phase.

2.3. R. opacus cultures for targeted metabolomics and transcriptomics

For phenotyping of adapted strains outside of adaptation conditions (Figs. 4A, C), targeted metabolomics experiments (Fig. 4B), and transcriptomic experiments (Figs. 5, 6), cultures were started as follows. − 80 °C frozen stocks of isolated colonies were streaked onto TSB agar plates and grown at 30 °C for three days. Using a loopful of cells from a TSB plate, seed cultures were grown at 30 °C in 2 mL of minimal medium A or B supplemented with lignin model compounds (0.2 g/L of BEN, GUA, PHE, HBA, and VAN, 1 g/L total aromatics) as carbon sources for 24 h, and then subcultured in 10 mL of the same media for 24 h with an initial cell density (OD_{600}) of 0.05. Next, cells were centrifuged at 3000 *g* for 10 min and resuspended in minimal medium A or B without carbon or nitrogen sources, and experiments were performed at 30 °C with a 10 mL culture volume in a 50 mL glass culture tube with respective carbon source(s) (see below for concentrations) and 1 g/L ammonium sulfate as the nitrogen source. For phenotyping of strains outside of adaptation conditions, 0.5 g/L of BEN, GUA, PHE, HBA, and VAN (2.5 g/L total aromatics), 0.6 g/L of BEN, GUA, PHE, HBA, and VAN (3.0 g/L total aromatics), or a combination of aromatics and glucose were used as carbon sources (at concentrations as indicated in figure captions). For targeted metabolomics experiments, 0.5 g/L of BEN, GUA, PHE, HBA, and VAN (2.5 g/L total aromatics) were used as carbon sources. For growth assays using individual compounds as sole carbon sources, six different concentrations of BEN (5, 6, 7, 8, 9, and 10 g/L), GUA (1.25, 1.5, 1.75, 2, 2.25, and 2.5 g/L), PHE (0.75, 1, 1.25, 1.5, 1.75, and 2 g/L), HBA (2, 2.25, 2.5, 2.75, 3, and 3.25 g/L), and VAN (1.25, 1.5, 1.75, 2, 2.25, and 2.5 g/L) were used. For transcriptomic experiments, seven different growth media were used: 0.5 g/L of BEN, 0.5 g/L of GUA, 0.5 g/L of PHE, 0.5 g/L of HBA, 0.5 g/L of VAN, and 1 g/L of glucose; and 0.5 g/L of BEN, GUA, PHE, HBA, and VAN (2.5 g/L total aromatics). Carbon sources are listed in the respective figure or table. Growth was monitored using Abs_{600} as described previously.

2.4. DNA extraction and sequencing library preparation

DNA was extracted using a standard bead-beating, phenol-chloroform extraction methodology (Yoneda et al., 2016), and DNA concentrations were quantified using a Quant-iT PicoGreen dsDNA Assay Kit (Thermo Fisher Scientific). The DNA was prepared for sequencing using a Nextera Tagmentation Kit (Illumina) (Baym et al., 2015; Caruccio, 2011). Samples were barcoded using a KAPA HiFi HotStart ReadyMixPCR Kit (KAPA Biosystems). The resulting PCR products were cleaned using Agencourt AMPure XP Beads (Agencourt Bioscience Corporation) and stored at − 20 °C until use. For sequencing, samples were pooled together in equimolar ratios and diluted to a final DNA concentration of 10 nM using nuclease free water.

2.5. Genome sequencing and SNP analysis

For whole genome sequencing (Fig. 3), 20 μL of the pooled barcoded DNA samples were submitted for sequencing at the Center for Genome Sciences & Systems Biology, Washington University in St. Louis School of Medicine. Samples were paired-end sequenced using an Illumina Hi-Seq 2500 System. Raw Illumina paired-end reads were demultiplexed using barcodes and quality trimmed using Trimmomatic (Bolger et al., 2014). Trimmed reads were mapped to the Chinese Academy of Science reference genome of *R. opacus* (ASM59954v1) (Chen et al., 2014) with the updated RefSeq annotation (GCF_000599545.1) using Bowtie2 (Langmead and Salzberg, 2012). The resulting SAM files were converted to BAM files and indexed using SAMtools (Li et al., 2009). SNPs and INDELs were called using Pilon (Walker et al., 2014), and SNPs also appearing in the WT strain were removed using an in-house Python script before quality filtering using GATK (DePristo et al., 2011). Trimmed reads were also *de novo* assembled using SPAdes (Nurk et al., 2013), and the resulting genome assembly was used to confirm the presence or absence of SNPs using BLAST+ (Camacho et al., 2009). Additionally, *de novo* confirmed SNPs were compared to another reference genome from the Broad Institute (ASM23433v1) (Holder et al., 2011) to filter out SNPs that were identical to the Broad Institute reference genome. Gene Ontologies (Ashburner et al., 2000) were inferred with Blast2GO (Gotz et al., 2008) by finding the top 20 most similar protein sequences in the NCBI and UniProt Knowledgebase databases for every protein in the *R. opacus* genome using BLAST+ and InterProScan (Jones et al., 2014).

2.6. RNA extraction and rRNA depletion

RNA was extracted using a ZR Fungal/Bacterial RNA MiniPrep Kit (Zymo Research) and treated with TURBO DNase I (Ambion) for 30 min at 37 °C to remove DNA contamination. DNase-treated RNA was then cleaned using an RNA Clean & Concentrator Kit (Zymo Research). Samples were checked for DNA contamination by PCR amplification using primers specific to intergenic regions of the genome. Samples that were positive for DNA contamination were re-treated with TURBO DNase I and cleaned until no DNA was detected by PCR amplification. Next, RNA was quantified using a NanoVue Plus™ Spectrophotometer (Biochrom), and ribosomal RNA (rRNA) was depleted from total RNA using a Bacterial Ribo-Zero rRNA Removal Kit (Illumina). The resulting mRNA was converted to cDNA and barcoded using a reverse transcription protocol described previously (Yoneda et al., 2016). cDNA samples were pooled together in equimolar ratios and diluted to a final cDNA concentration of 10 nM using nuclease free water.

2.7. Transcriptomic analysis

For transcriptomic analysis of WT and PVHG6 strains (Figs. 5, 6), 20 μL of the pooled barcoded cDNA samples were submitted for sequencing at the Center for Genome Sciences & Systems Biology, Washington University in St. Louis School of Medicine. Samples were single-end sequenced using an Illumina Hi-Seq 2500 System. Raw single-end reads were demultiplexed, trimmed, and mapped in the same manner as the SNP analysis described previously. After indexing mapped reads, expression counts were calculated for each gene using featureCounts (Liao et al., 2014), and downstream differential gene expression analysis was performed using DESeq2 (Love et al., 2014).

2.8. Aromatic consumption profiling

For cultures using a single carbon source, the concentration of each lignin model compound was estimated by comparing UV absorbance values to a standard curve for each lignin model compound (Fig. 4C, Fig. S22). 200 μL of each cell culture was centrifuged at 16,000 *g* for 5 min, and the UV absorbance value of a 100-fold dilution of culture supernatant was measured in a UV transparent 96 well plate (Thermo Scientific) using a TECAN Infinite M200 Pro plate reader, or in a quartz cuvette using a Nanodrop 2000 (Thermo Scientific). For cultures using the aromatic mixture (Fig. 4B), aromatics in the culture supernatant were derivatized using methyl chloroformate (Madsen et al., 2016) and quantified using a custom GC-MS-FID system (gas chromatography-mass spectrometry-flame ionization detector). Briefly, the culture supernatant was centrifuged at 16,000 *g* for 5 min, and 200 μL of the culture supernatant was mixed with 40 μL of 5.0% (w/w) sodium hydroxide solution, 200 μL of methanol, and 50 μL of pyridine. Methyl chloroformate (50 μL) was added to the mixture in two 25 μL aliquots. Next, 400 μL of chloroform containing a decane internal standard was added to the sample, followed by the addition of 400 μL of 50 mM sodium bicarbonate solution to induce phase separation of the aqueous and organic layers. Samples were vortexed between each step to ensure complete mixing. After phase separation, the organic phase was transferred to a GC vial with a 350 μL glass insert (Agilent), and samples were analyzed using an Agilent 7890A GC coupled to both an Agilent 5975C mass spectrometer containing a triple-axis detector and an Agilent G3461A FID detector with a methanizer (Activated Research Company). The Agilent 7890A GC was equipped with a Restek fused silica RTX-50 capillary column (30 m by 0.25 mm, 0.5 μm film thickness), and helium was used as the carrier gas. 1 μL of the organic phase was injected with a splitting ratio of 10:1 using the autosampler. For GC runs, the inlet was maintained at 250 °C, and the oven was held for 2 min at 40 °C, heated to 300 °C using a 5 °C/min ramp, and held at 300 °C for 5 min. All data was exported and analyzed using the Agilent ChemStation Software, and peak intensities were normalized to the decane internal standard. Lignin model compounds were identified based on retention time and mass spectral database searches using the Palisade Complete Mass Spectral Database (600 K edition, Palisade Mass Spectrometry, Ithaca, NY), and concentrations were determined using an external standard curve for each lignin model compound.

2.9. Lipid assay

For lipid production assays (Fig. 7), growth experiments were performed in the same way as metabolomic and transcriptomic experiments with the following modification: the culture volume was 50 mL in a 250 mL baffled flask, the carbon sources for the experiment were 0.5 g/L of BEN, GUA, PHE, HBA, and VAN (2.5 g/L total aromatics), and the nitrogen source for the experiment was 0.125 g/L ammonium

sulfate. Lipid was measured gravimetrically using a modified Folch lipid extraction (Folch et al., 1957). To measure biomass content, 10 mL of cell culture was centrifuged at 4600 *g* for 15 min, washed twice with distilled water, dried at 60 °C for two days, and weighed to determine the dry cell weight. For lipid extractions, 30 mL of cell culture was centrifuged at 4600 *g* for 15 min, washed twice with distilled water, and resuspended in 4 mL of a chloroform/methanol solution (2:1). Next, the solution was sonicated at 20% amplitude using the program: 1 s on and 1 s off for 5 min. The solution was partitioned into aqueous and organic phases using 0.2 volumes of 0.9% NaCl solution. The organic phase was separated from the aqueous phase, dried under vacuum, and weighed to determine the total lipid amount.

2.10. Generation of R. opacus knockout mutants

Knockout mutants were generated via homologous recombination in the wild type *R. opacus* strain as described previously (DeLorenzo et al., 2018). Briefly, a helper plasmid expressing a pair of recombinases (pDD120) was introduced via electroporation into WT *R. opacus*. Electrocompetent cells were made from this strain as previously described (DeLorenzo et al., 2017). An integration vector containing an antibiotic resistance marker and DNA regions homologous to each target gene (~ 500 bp per homologous arm) was then introduced into the strain harboring the recombinase helper plasmid by electroporation (DeLorenzo et al., 2018). Successful recombination was confirmed by colony PCR. See Table S16 for plasmids utilized for knockouts and Table S17 for all strains generated. Plasmid DNA was isolated from *Escherichia coli* DH10B for electroporation into *R. opacus* using the Zyppy Plasmid Miniprep Kit (Zymo).

3. Results

3.1. Adaptive evolution and characterization of adapted strains

To determine *R. opacus*' ability to improve its aromatic tolerance and consumption, we adaptively evolved it using increasingly higher concentrations of individual lignin model compounds and combinations of lignin model compounds (a total of 32 conditions without added sugars, Fig. 1, Table S1). For comparison to aromatic adaptation experiments, we also serially passaged *R. opacus* using high concentrations of glucose. For further analysis, we selected four adaptation experiments that used one to four different lignin model compounds that included phenol and other phenolic compounds as carbon sources, as well as two adaptation experiments that used sodium benzoate (a non-phenolic lignin model compound) and glucose as sole carbon sources. The adaptation experiments chosen for further characterization were: 1) phenol (P); 2) phenol and vanillate (PV); 3) phenol, vanillate, and 4-hydroxybenzoate (PVH); 4) phenol, vanillate, 4-hydroxybenzoate, and guaiacol (PVHG); 5) sodium benzoate (B); and 6) high glucose. Six colonies from each of these six chosen adaptation experiments were isolated, and their growth was compared to that of the WT strain using their respective adaptation carbon source(s) (Figs. 2, S1). 35 of the 36 isolated strains had significantly higher cell densities (OD_{600}; up to 1900% improvement) than the WT strain after 43 h of growth on the carbon sources used in their adaptation. Aromatic consumption patterns for adapted strains after 43 h of growth suggest that improved growth of these strains is due to both consumption of and tolerance to aromatic carbon sources (Fig. S2). These results demonstrate that *R. opacus* can be adaptively evolved to improve growth on different combinations of lignin model compounds.

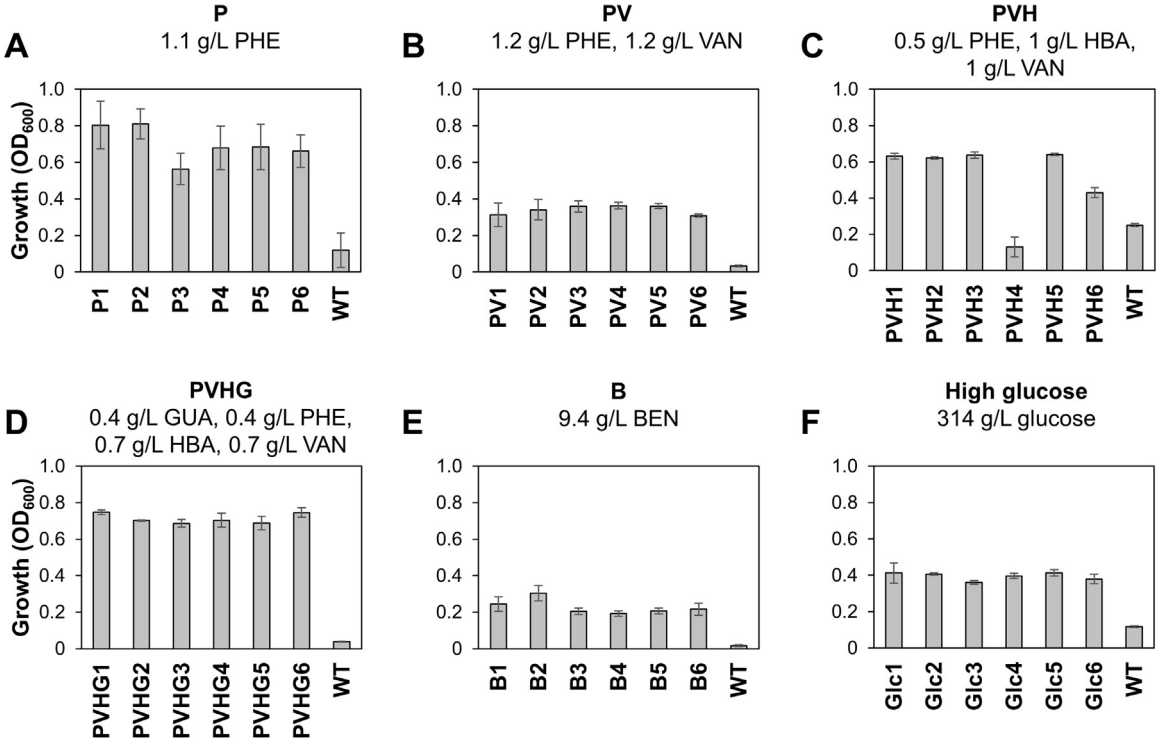

Fig. 2. Growth of the WT strain and adapted strains using adaptation carbon sources. Bars represent OD_{600} values measured at 43 h of growth in minimal medium A supplemented with the listed carbon sources and 1 g/L ammonium sulfate as the nitrogen source. A. The PHE adapted strains (P1–6) compared to the WT strain using 1.1 g/L PHE. B. The PHE and VAN adapted strains (PV1–6) compared to the WT strain using 1.2 g/L PHE and 1.2 g/L VAN. C. The PHE, VAN, and HBA adapted strains (PVH1–6) compared to the WT strain using 0.5 g/L PHE, 1 g/L HBA, and 1 g/L VAN. D. The PHE, VAN, HBA, and GUA adapted strains (PVHG1–6) compared to the WT strain using 0.4 g/L GUA, 0.4 g/L PHE, 0.7 g/L HBA, and 0.7 g/L VAN. E. The BEN adapted strains (B1–6) compared to the WT strain using 9.4 g/L BEN. F. The high glucose adapted strains (Glc1–6) compared to the WT strain using 314 g/L glucose. Bars represent the average of three biological replicates and error bars represent one standard deviation. PHE = phenol, VAN = vanillate, HBA = 4-hydroxybenzoate, GUA = guaiacol, and BEN = sodium benzoate.

3.2. Comparative genomics of adapted strains

To identify possible causative mutations for adaption, we examined the 35 isolated strains with improved growth (Fig. 2) by whole genome sequencing (> 38× coverage per strain). Across all 35 strains, genomic analysis revealed a total of 255 distinct SNPs and 6 insertion/deletions (INDELs) distributed over the chromosome and 6 of the 9 endogenous plasmids (Chen et al., 2014) (Fig. S3, Tables S2–S4). Based on sequencing depth, we observed major deletions in Plasmid 1 for 11 strains from the PVHG, B, and high glucose adaptation experiments, and we observed complete loss of Plasmid 2 in 25 strains from the P, PV, PVH, PVHG, and B adaptation experiments (Fig. S4). Plasmids 1 and 2 are large plasmids with sizes of 172,218 bp and 97,588 bp, respectively. Growth improvements could result from either deletion of burdensome genes, reduced replication costs for maintaining large plasmids, or a combination of both (Dionisio et al., 2005; Harrison and Brockhurst, 2012).

To identify potential common patterns of genetic changes between strains and adaptation conditions, we classified genes affected by mutations using Gene Ontology (GO) terms (Ashburner et al., 2000) and then further grouped GO terms into broader functional categories (Fig. 3A). Interestingly, many genes involved in redox reactions were affected by SNPs after adaptation in phenolic compound mixtures (Fig. 3A). On average, 36% of the non-synonymous SNPs in strains adapted using phenolic compounds, compared to only 16% in strains adapted using non-phenolic carbon sources (e.g., BEN and glucose), were found in genes related to redox reactions. These results suggest that the selection pressure applied by adaptive evolution targeted redox reactions to improve tolerance and utilization of phenolic compounds.

We identified seven genes that were affected by non-synonymous SNPs across multiple aromatic adaptation experiments (Fig. 3B, Table S5). Surprisingly, we did not observe any shared genes whose annotation is related to aromatic degradation. Of the seven genes, three genes are annotated to be involved in redox reactions: RS14825 (cytochrome ubiquinol oxidase subunit I), RS01890 (manganese-dependent superoxide dismutase [SOD]), and RS38570 (a FAD-binding oxidoreductase). Non-synonymous or intergenic SNPs affecting cytochrome ubiquinol oxidase and superoxide dismutase were found in at least one strain from all four adaptation experiments containing phenolic compounds, but not in any strains from the B and high glucose adaptation experiments. The previous adaptation experiment in *R. opacus* using phenol (Yoneda et al., 2016) also led to a mutation in cytochrome ubiquinol oxidase. Furthermore, two genes involved in gluconeogenesis had non-synonymous SNPs in multiple adaptation lineages: RS08140 (phosphoenolpyruvate [PEP] carboxykinase) and RS10095 (class II fructose-bisphosphate aldolase). Additionally, two genes related to phosphorylation had non-synonymous SNPs: RS32480 (phosphotransferase) and RS39015 (serine/threonine protein kinase).

To investigate the consequence of non-synonymous SNPs in the cytochrome ubiquinol oxidase and SOD genes further, we modeled the mutational sensitivity (i.e., the probability of the mutation having a phenotypic effect) using Phyre2 (Kelley et al., 2015) and SUSpect (Yates et al., 2014). The modified residues in the adapted strains for both genes had mutational sensitivities ranging from medium to very high for the modified amino acids, suggesting that these SNPs could have a phenotypic effect (either positive or negative; Tables S6, S7) (Yates et al., 2014). To verify the modeling results for superoxide dismutase, we measured the SOD activity using cell lysates from the WT strain and one of our multi-compound adapted strains with a non-synonymous SNP in SOD (PVHG6). The adapted PVHG6 strain showed a 56% lower SOD activity compared to that of the WT strain (Fig. S5). This lower activity suggests that the adapted strain is likely to reduce fewer superoxide radicals than the WT strain, which could contribute to its improved growth in the mixture of lignin model compounds through

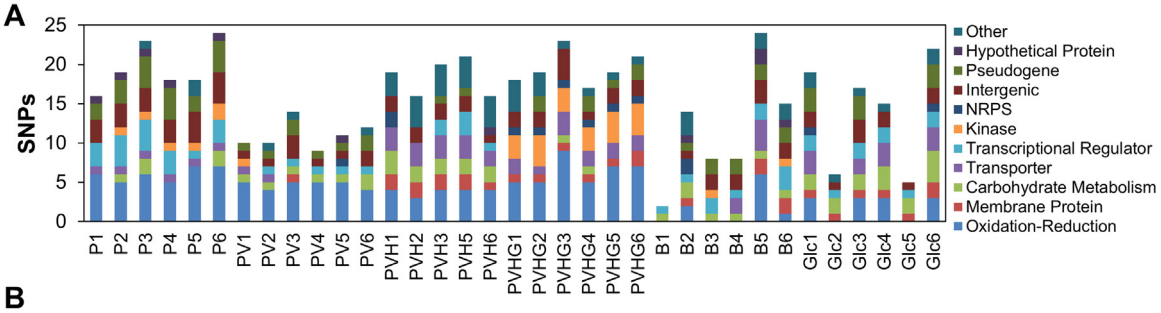

B

Strains	Gene ID	Annotation	Location	Base Mean Expression
All P, All PV, PVH6, All PVHG	RS01890	superoxide dismutase	Chromosome	32,010
All B, All PVH	RS08140	phosphoenolpyruvate carboxykinase	Chromosome	30,198
P2, P3, P6, All PV	RS10095	class II fructose-bisphosphate aldolase	Chromosome	5,291
All P, All PV, All PVH, All PVHG	RS14825	cytochrome ubiquinol oxidase subunit I	Chromosome	23,629
PV3, All PVHG	RS32480	phosphotransferase	Chromosome	285
P5, PV3, PVH3, PVH5, B6	RS38570	FAD-binding oxidoreductase	Plasmid 1	60
P2, P3, P4, P5, P6, All PVHG	RS39015	serine/threonine-protein kinase PknK	Plasmid 3	354

Fig. 3. Comparative genomics of lignin model compound adapted strains. A. Categorization of genes with non-synonymous SNPs or intergenic SNPs that could affect gene expression using Gene Ontology (GO) terms organized by strain. Strain names indicate the adaptation condition from which each strain originated: P = phenol; PV = phenol and vanillate; PVH = phenol, vanillate, and 4-hydroxybenzoate; PVHG = phenol, vanillate, 4-hydroxybenzoate, and guaiacol; B = sodium benzoate; and Glc = glucose. See Supplementary information for all SNP information, including silent SNPs. B. Genes with non-synonymous SNPs or intergenic SNPs that could affect gene expression and that were found across multiple aromatic adaptation experiments. Putative annotations are from NCBI reference sequence NZ_CP003949.1. "All" indicates that all sequenced strains isolated from the indicated adaptation condition contain either non-synonymous SNPs or intergenic SNPs that could affect gene expression. Base Mean Expression is the average of the normalized counts from WT and PVHG6 transcriptomic data from all growth conditions.

their facilitated oxidation (Bugg, 2001; Gatti et al., 1994).

3.3. Characterization of adapted strains on lignin model compound mixtures

Efficient microbial lignin valorization requires the utilization of complex aromatic compound mixtures. Thus, we sought to determine the performance of our aromatic adapted strains in mixtures of lignin model compounds compared to the WT strain. We hypothesized that the adapted strains' improved tolerance phenotype towards a subset of five chosen lignin model compounds (one to four compounds) could be extended to a mixture of all five compounds. To test this hypothesis, we grew one strain from each of the P, PV, PVH, PVHG, and B adaptation experiments on a mixture of five aromatics (PHE, GUA, HBA, VAN, and BEN). At 2.5 g/L total aromatics (0.5 g/L of each lignin model compound), all five adapted strains had significantly higher growth rates than the WT strain ($P < 0.009$ for all adapted strains; Fig. 4A, Table S8). P1, PV1, and PVHG6 strains reached a higher OD_{600} than the WT strain after 100 h of growth ($P < 0.004$ for all three strains), while PVH5 and B2 did not reach significantly higher OD_{600} values (Table S8). PVHG6 reached the highest OD_{600} among all strains after 70 h of growth, which was 96% higher than the WT strain ($P = 3.8 \times 10^{-6}$). At 3.0 g/L total aromatics (0.6 g/L of each aromatic compound), all strains had significantly higher growth rates than the WT strain ($P < 0.03$ for all adapted strains; Fig. S6, Table S9). P1, PV1, and PVHG6 also reached 75–85% higher OD_{600} values than the WT strain after 100 h of growth ($P < 0.03$ for all three strains), while PVH5 and B2 did not reach significantly higher OD_{600} values (Fig. S6, Table S9). These results demonstrate that some adapted strains (P1, PV1, and PVHG6) have improved growth on a mixture of aromatics, some of which were not used during their adaptation. For the three best-performing strains (P1, PV1, and PVHG6), the only exclusively shared gene which was affected by a SNP was SOD (Fig. 3B), which further supports that SOD may be related to improved growth on lignin model compounds. Because PVHG6 showed the best growth performance at both 2.5 and 3.0 g/L total aromatics, it was chosen for further characterization.

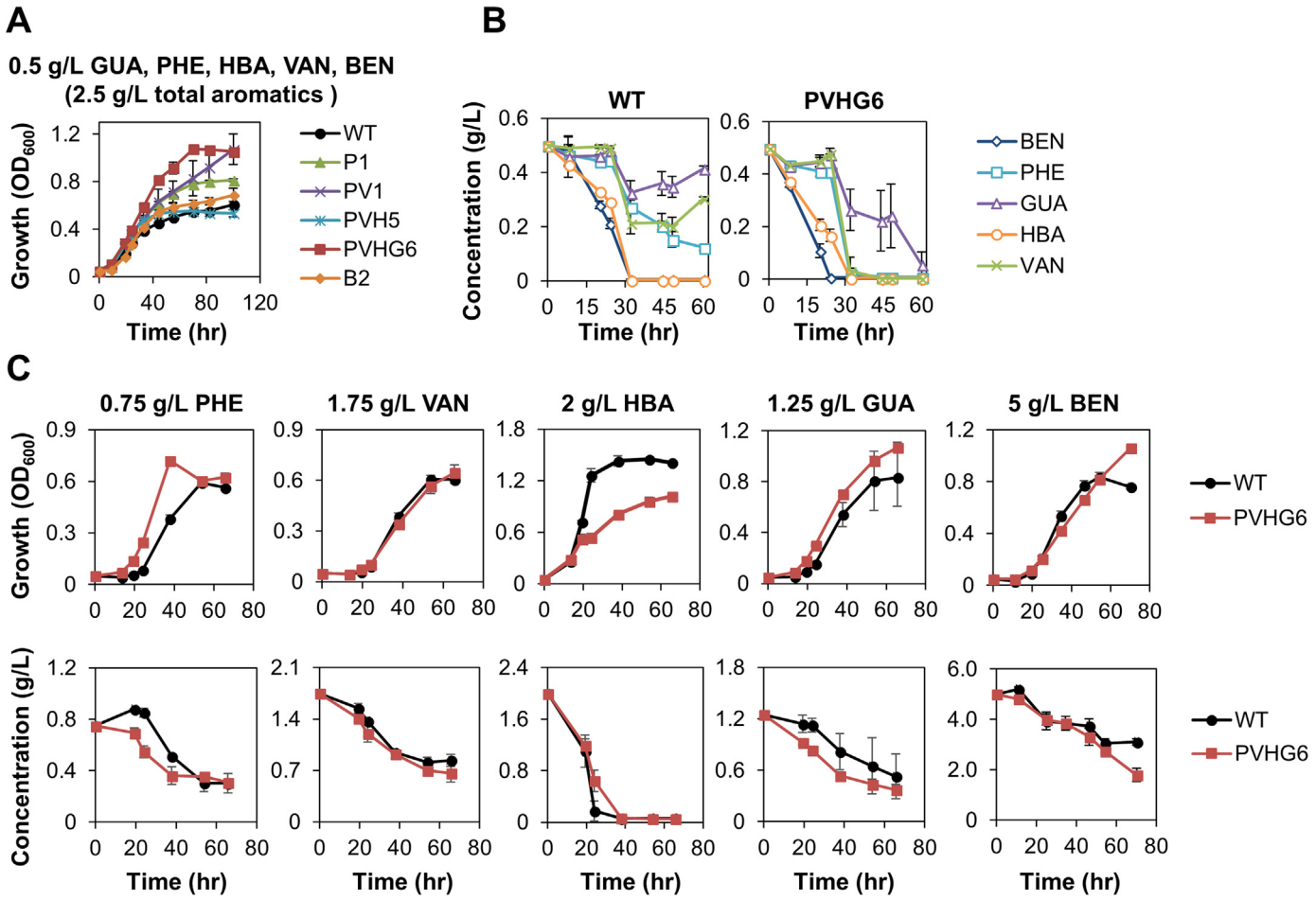

Fig. 4. Growth and consumption of lignin model compounds by WT and adapted strains. Cells were grown in minimal medium A supplemented with the listed carbon sources and 1 g/L ammonium sulfate as the nitrogen source. A. Growth of one strain from each aromatic adaptation experiment and the WT strain in a mixture of lignin model compounds (0.5 g/L each of GUA, PHE, HBA, VAN, and BEN; 2.5 g/L total aromatics). B. Aromatic consumption profiles of WT and PVHG6 strains in the same growth condition as A. Aromatic concentrations were measured by derivatizing culture supernatants using methyl chloroformate followed by GC-MS-FID (see Section 2 for details). C. Growth and consumption of individual aromatic compounds as a sole carbon source by WT and PVHG6 strains (aromatic concentrations listed above plots). Aromatic concentrations were estimated using UV absorbance (see Section 2 for details). Note that the y-axis scales for growth and concentration plots vary between carbon sources. For all plots, points represent the average of three biological replicates and error bars represent one standard deviation. PHE = phenol, VAN = vanillate, HBA = 4-hydroxybenzoate, GUA = guaiacol, and BEN = sodium benzoate.

3.4. Aromatic consumption in a lignin model compound mixture by PVHG6

Next, we sought to determine if all lignin model compounds in the five-compound mixture were used for growth and if PVHG6 consumed aromatics in a similar manner to that of the WT strain. We used a targeted metabolomic approach to measure the concentration of each individual aromatic compound in the mixture (0.5 g/L of PHE, GUA, HBA, VAN, and BEN; 2.5 g/L total aromatics; Fig. 4B). We observed that both WT and PVHG6 strains consumed BEN and HBA before PHE, GUA, and VAN. Both strains fully consumed BEN and HBA within 24–32 h, while consumption of PHE, GUA, and VAN began after 24 h for both strains. Within 60 h, all five compounds were almost fully consumed by the PVHG6 strain, but substantial amounts of PHE (25%), GUA (83%), and VAN (61%) remained in the WT cultures at 60 h. Overall, PVHG6 had a 27% higher total aromatic consumption rate than the WT strain (52 mg/L/h for PVHG6 vs. 41 mg/L/h for the WT strain from 0 to 44 h, $P = 0.0024$). Additionally, it was found that PVHG6 also consumed a mixture containing 3 g/L glucose and all five aromatic compounds (0.6 g/L of PHE, GUA, HBA, VAN, and BEN; 3 g/L total aromatics) as carbon sources, and it completely utilized all aromatics after 60 h of growth (Fig. S7).

3.5. Consumption of individual aromatic compounds by PVHG6

To determine whether the improved growth phenotype of PVHG6 on a mixture of lignin model compounds extended to individual compounds, we measured growth and aromatic concentrations using six different concentrations of PHE, VAN, HBA, GUA, and BEN as a sole carbon source (Figs. 4C, S8–S13). Aromatic concentrations were measured using UV absorbance. From these experiments, we calculated the half maximal inhibitory concentration (IC_{50}) using OD_{600} values at 54 h. We only observed a significant increase in the IC_{50} value of PVHG6 compared to that of the WT strain when they were grown in PHE (17%, $P = 0.003$) and GUA (16%, $P = 0.008$) (Table S10). The IC_{50} values of PVHG6 for HBA, VAN, and BEN were unchanged or slightly decreased (Table S10). When 1 g/L glucose was used as a sole carbon source, no difference in growth was observed between the WT and PVHG6 strains (Fig. S14), implying that glucose metabolism was not affected by mutations during the long adaptation process in the absence of glucose.

3.6. Transcriptomic analysis of WT and PVHG6 using lignin model compounds

We had previously observed that changes in gene and pathway expression better explained improved phenol utilization phenotypes in evolved *R. opacus* strains, compared to the effect of genetic changes like SNPs and INDELs in coding regions (Yoneda et al., 2016). Accordingly, we sought to determine the potential role of transcriptional differences in the improved tolerance and utilization of a larger panel of aromatics by the evolved PVHG6 strain. We performed whole cell gene expression profiling via RNA-Seq on the WT and PVHG6 strains grown in a mixture of all five lignin model compounds (0.5 g/L of each lignin model compound, 2.5 g/L total aromatics), or in 1 g/L glucose, to identify differentially regulated genes between strains and carbon sources (Table S11). We also performed RNA-Seq using 0.5 g/L of each of the five lignin model compounds individually (PHE, GUA, HBA, VAN, or BEN) to determine compound-specific degradation pathways for each compound (Table S11). For the 1 g/L glucose (Glc) and the mixture of five lignin model compounds (hereafter, “mixture”), we analyzed the transcriptome at both the early and mid-exponential phases (20 h and 32 h for the mixture; 10 h and 13 h for Glc) since we had observed differential consumption rates of lignin model compounds in our targeted metabolomic analysis (Fig. 4B).

3.6.1. Principal component analysis of transcriptomic data and comparison of differentially upregulated genes between PVHG6 and WT strains

To investigate differences in expression profiles between WT and PVHG6, we first analyzed all transcriptomic data for both strains using principal component analysis (Fig. S15). PVHG6 and WT were clearly separated along the first principal component with values higher than 60 and lower than −50, respectively, while the second principal component generally separated transcriptional profiles by growth conditions. Permutational ANOVA (PERMANOVA) indicated that transcriptomic profiles between strains and between growth conditions were significantly different ($P = 0.001$, both cases). Based on our genome sequencing data, which was corroborated by our transcriptomic data (Fig. S4), many adapted strains, including PVHG6, underwent plasmid deletions and plasmid loss. We repeated the principal component analysis with Plasmid 1 and 2 data removed, and while some growth conditions led to closer visual clustering of WT and PVHG6, the strains were still significantly different based on PERMANOVA ($P = 0.002$; Fig. S16).

We then compared the top 30 differentially upregulated genes between both strains grown in the mixture at both time points (Fig. S17). The most upregulated genes in PVHG6 relative to the WT strain in the mixture at both time points were RS27075 (a hypothetical protein, 41-fold upregulated) and RS13410 (a type VII secretion-associated protein, 40-fold upregulated), respectively. Five of the top 30 upregulated genes are annotated as ABC transporters or ABC transporter associated proteins, suggesting that these ABC transporters might control uptake or export rates of aromatic compounds. Two genes annotated as acetyl-CoA acetyltransferases (RS34095 and RS34105) were also in the top 30 list. Both proteins share high positive amino acid sequence similarity to 3-oxoadipyl-CoA thiolases in *R. opacus* and *R. jostii* RHA1 (52–76% positive identity, Table S12). The final step in the β-ketoadipate pathway is catalyzed by 3-oxoadipyl-CoA thiolase, converting 3-oxoadipyl-CoA into succinyl-CoA and acetyl-CoA. RS34095 and RS34105 may encode this enzyme, acting as additional gene copies and increasing the metabolic flux through the β-ketoadipate pathway in PVHG6 when the aromatic mixture is used.

3.6.2. Lignin model compound funneling pathways

To identify putative funneling pathway enzymes for each lignin model compound, we searched for the most strongly upregulated enzymes when both strains were grown in the individual aromatic compounds and the mixture, compared to the glucose condition (Fig. 5A, Table S11). These selected proteins were then compared to homologous enzymes in a closely-related strain, *R. jostii* RHA1, which has a characterized proteome (Patrauchan et al., 2012) (Table S13). Using this process, we identified funneling pathway clusters for each lignin model compound: two two-component phenol hydroxylases (RS31555–RS31560 and RS30765–RS30770), a putative vanillate demethylase (RS02665–RS02675), a putative 4-hydroxybenzoate monooxygenase (RS31675), two putative cytochrome P450 clusters upregulated in response to GUA (RS30780–RS30785 [GUA degradation cluster #1] and RS21470–RS21485 [GUA degradation cluster #2]), and a putative benzoate degradation cluster (RS30790–RS30805). Many of these funneling pathway enzymes have high sequence similarity to biochemically characterized pathway enzymes in other *Rhodococcus* strains, including *R. opacus* 1CP (Table S13) (Gröning et al., 2014; Solyanikova et al., 2016). Each of these genes or gene clusters converts lignin model compounds to either catechol (CAT) or protocatechuate (PCA) for subsequent degradation by the β-ketoadipate pathway (Fig. 6B). All of these genes were upregulated in both the individual aromatic condition and the mixture compared to glucose, except GUA degradation cluster

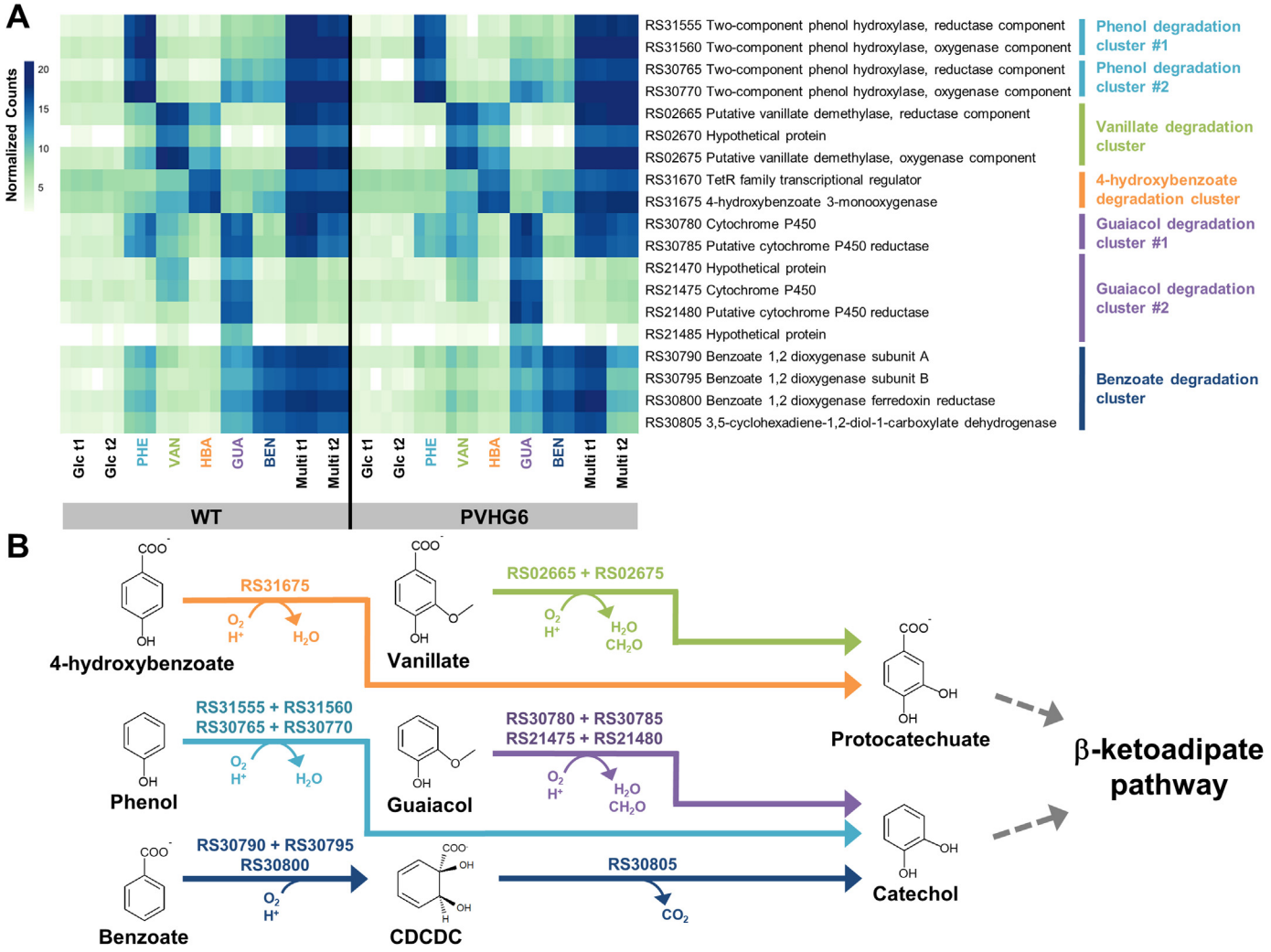

Fig. 5. Activation of lignin model compound funneling pathways in *R. opacus*. A. Heat map of normalized expression counts for upregulated aromatic degradation genes that convert (i.e. "funnel") lignin model compounds to the β-ketoadipate pathway during growth on individual lignin model compounds, a mixture of lignin model compounds, and glucose. Raw counts were transformed using the variance stabilizing transformation in DESeq2. Darker colors indicate higher normalized counts (see scale bar). Glc = 1 g/L glucose, PHE = 0.5 g/L phenol, VAN = 0.5 g/L vanillate, HBA = 0.5 g/L 4-hydroxbenzoate, GUA = 0.5 g/L guaiacol, BEN = 0.5 g/L sodium benzoate, and Multi = 0.5 g/L of PHE, VAN, HBA, GUA, and BEN (2.5 g/L total aromatics). t_1 represents cells harvested at early exponential phase (10 h for Glc; 20 h for Multi), while t_2 represents cells harvested at mid-exponential phase (13 h for Glc; 32 h for Multi). Samples from individual compound growth conditions were harvested at mid-exponential phase (24 h for WT PHE, 21 h for PVHG6 PHE, 19 h for WT and PVHG6 GUA, 11 h for WT and PVHG6 HBA, 12 h for WT and PVHG6 BEN, 24 h for WT and PVHG6 VAN). Cells were grown in minimal medium A. Each square on the heat map represents a biological replicate. B. Pathway map showing genes involved in lignin model compound funneling pathways in *R. opacus*. Gene codes are from the NCBI reference sequence NZ_CP003949.1. CDCDC = cis-1,2-dihydroxy-cyclohexa-3,5-diene-1-carboxylate.

#2 which was upregulated in GUA but not upregulated in the mixture compared to glucose (Fig. 5A). This differential expression suggests transcriptional regulation (i.e., repression) of this funneling pathway in response to the presence of other lignin model compounds. When the expression of the identified funneling pathways in PVHG6 was compared to the WT strain in the mixture, most genes at both time points were not differentially expressed with the exception of the benzoate degradation pathway at the second time point, which was 29–95-fold downregulated (adjusted p-values $< 7 \times 10^{-29}$, Table S11). Our metabolomic data (Fig. 4B) showed that PVHG6 completely consumed BEN after 24 h (compared to 32 h for WT), which suggests that the BEN funneling pathway genes were downregulated in PVHG6 in response to complete consumption of BEN. For other funneling pathways, no genes were more than 2.6-fold upregulated or downregulated in PVHG6 compared to the WT strain at either time point in the mixture (Table S11).

3.6.3. *Expression of β-ketoadipate pathways during lignin model compound consumption*

The funneling pathways convert aromatic compounds into two intermediates, CAT or PCA, for degradation by the β-ketoadipate pathway (Fig. 6). Previous analyses of *Rhodococcus* strains suggest that VAN and HBA are converted to PCA, while GUA, BEN, and PHE are converted to CAT (DeLorenzo et al., 2017). For both WT and PVHG6, we observed upregulation of β-ketoadipate gene cluster #1 (RS25340–RS25375) compared to the glucose condition for all aromatic carbon sources

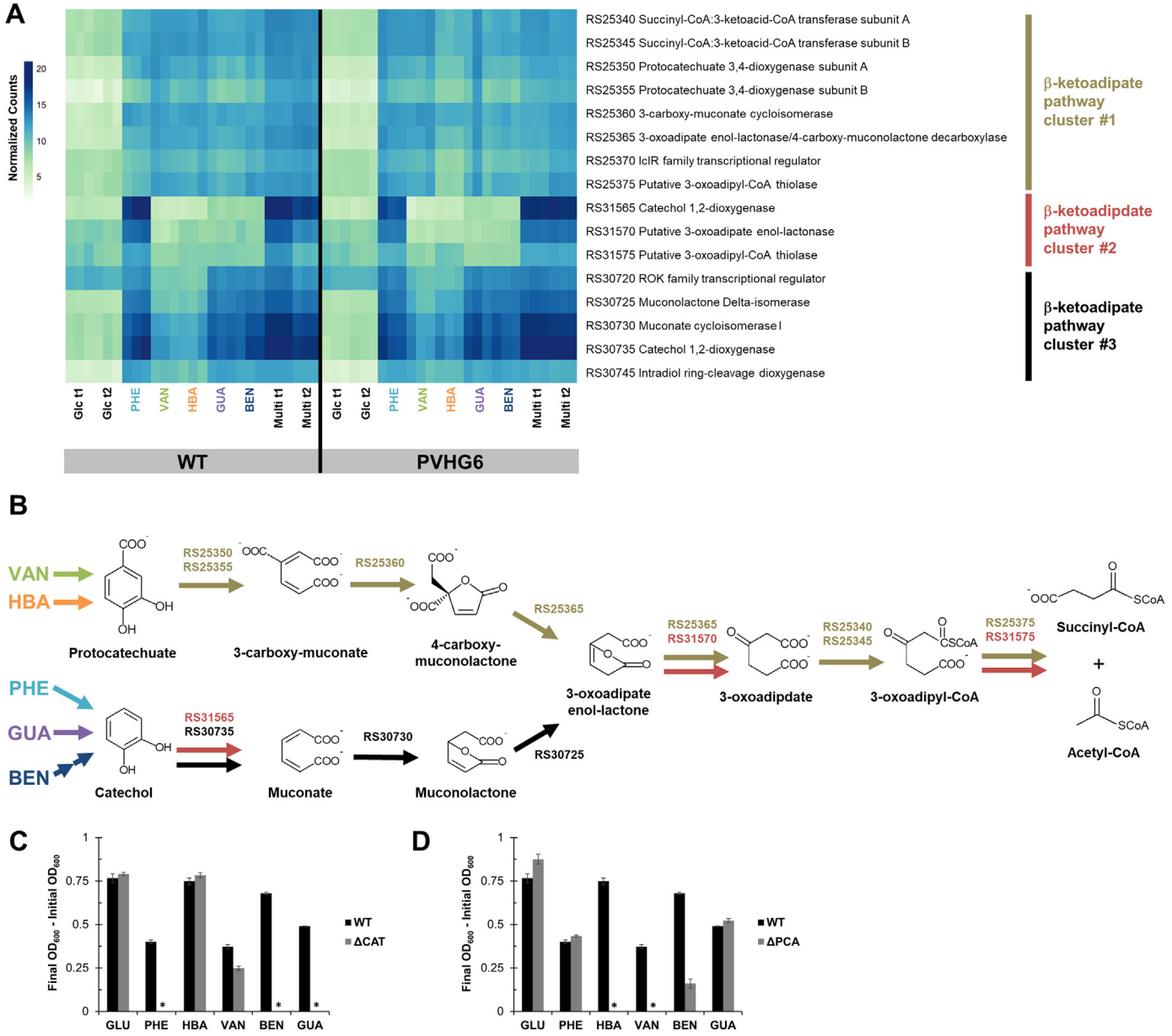

Fig. 6. Activation of β-ketoadipate pathway gene clusters by lignin model compounds in *R. opacus*. A. Heat map of normalized gene expression counts for β-ketoadipate pathway gene clusters during growth on individual lignin model compounds, a mixture of lignin model compounds, and glucose. Raw counts were transformed using the variance stabilizing transformation in DESeq2. Darker colors indicate higher normalized counts (see scale bar). Glc = 1 g/L glucose, PHE = 0.5 g/L phenol, VAN = 0.5 g/L vanillate, HBA = 0.5 g/L 4-hydroxbenzoate, GUA = 0.5 g/L guaiacol, BEN = 0.5 g/L sodium benzoate, and Multi = 0.5 g/L of PHE, VAN, HBA, GUA, and BEN (2.5 g/L total aromatics). t_1 represents cells harvested at early exponential phase (10 h for Glc; 20 h for Multi), while t_2 represents cells harvested at mid-exponential phase (13 h for Glc; 32 h for Multi). Samples from individual compound growth conditions were harvested at mid-exponential phase (24 h for WT PHE, 21 h for PVHG6 PHE, 19 h for WT and PVHG6 GUA, 11 h for WT and PVHG6 HBA, 12 h for WT and PVHG6 BEN, 24 h for WT and PVHG6 VAN). Cells were grown in minimal medium A. Each heat map square represents a biological replicate. B. Pathway map showing genes involved in β-ketoadipate pathway gene clusters in *R. opacus*. Gene codes are from the NCBI reference sequence NZ_CP003949.1. C. Difference between initial OD_{600} and final OD_{600} after 24 h of growth for the RS30730 knockout (ΔCAT) strain and the WT strain using different carbon sources. D. Difference between initial OD_{600} and final OD_{600} after 24 h of growth for the RS25360 knockout (ΔPCA) strain and the WT strain using different carbon sources. For C and D, the WT, ΔCAT, and ΔPCA strains were initially cultured in 2 mL of minimal medium B containing 1 g/L ammonium sulfate, 4 g/L glucose, and either no aromatic compound, 0.2 g/L PHE, 0.25 g/L GUA, 0.5 g/L HBA, 0.25 g/L VAN, or 0.5 g/L BEN. Cells were then centrifuged, washed with minimal medium B containing no carbon source, and re-suspended to an initial OD_{600} of 0.2 in 10 mL of minimal medium B containing 1 g/L ammonium sulfate and either 1 g/L glucose, 0.4 g/L PHE, 0.5 g/L GUA, 1.0 g/L HBA, 0.5 g/L VAN, or 1 g/L BEN as sole carbon sources. Asterisk (*) indicates that the difference between initial and final OD_{600} values is less than one standard deviation. Bars represent the average of three biological replicates and error bars represent one standard deviation.

(Fig. 6A, Table S11). This gene cluster includes genes required to convert both CAT and PCA into central tricarboxylic acid (TCA) cycle metabolites. In both strains, β-ketoadipate gene cluster #2 (RS31565–RS31575) was upregulated in PHE and the mixture (up to 5000-fold), but it was upregulated only up to 3-fold in other lignin model compounds compared to the glucose condition (Table S11). This observed upregulation could be related to the upstream phenol hydroxylase (RS31555–RS31560 in the phenol funneling pathway; Fig. 5A) that is highly upregulated in PHE compared to the glucose condition. We also observed upregulation of β-ketoadipate gene cluster

#3 (RS30720–RS30745) during growth on all aromatic carbon sources. In both strains, genes in this cluster, which is typically associated with degradation of CAT intermediates, were highly upregulated (142–779-fold) by CAT branch compounds (GUA, BEN, and PHE) relative to the glucose condition, but they were only moderately upregulated (9–93-fold) by PCA branch compounds (VAN and HBA) relative to the glucose condition (Table S11). Interestingly, such a branch-dependence was also observed in regulation of some funneling enzymes (Fig. 5A). For example, a phenol hydroxylase (RS30765–RS30770) was also highly upregulated in GUA (121–477-fold), but minimally upregulated by PCA precursors VAN and HBA (up to 5.9-fold), compared to the glucose condition in both strains (Table S11). The putative vanillate demethylase (RS02665–RS02675) was also upregulated in HBA (114–295-fold), but minimally upregulated by CAT precursors GUA and BEN (1.4–2.2-fold) in both WT and PVHG6, compared to the glucose condition (Table S11). When compared to the WT strain in the mixture, PVHG6 did not show substantial upregulation of the β-ketoadipate clusters (at most 2.5-fold) (Table S11). This result differs from that of previously characterized *R. opacus* mutants that were adapted using a single compound (PHE) and that showed large differential upregulation of a number of phenol degradation genes in PHE compared to the WT strain (Yoneda et al., 2016).

To confirm whether the five tested aromatic compounds (PHE, GUA, HBA, VAN, and BEN) were catabolized via the CAT or PCA branch of the β-ketoadipate pathway, critical genes from both branches were knocked out, and growth assays were performed. β-ketoadipate gene cluster #3, which contains the CAT degradation pathway, was knocked out by a disruption of RS30730 (cis,cis-muconate cycloisomerase; ΔCAT), while β-ketoadipate gene cluster #1, which contains the PCA degradation pathway, was knocked out by a disruption of RS25360 (3-carboxy-cis,cis-muconate cycloisomerase; ΔPCA). The knockout of the PCA degradation pathway was complicated by the fact that other central β-ketoadipate pathway genes required for CAT degradation are located further downstream in β-ketoadipate gene cluster #1 (Fig. 6). To ensure transcription of those downstream genes, a constitutive promoter was integrated into the genome. The ΔCAT strain was unable to grow using PHE, GUA, and BEN as sole carbon sources, while the ΔPCA strain was unable to grow using HBA and VAN as sole carbon sources (Figs. 6C, 6D). Together, these results confirm that PHE, GUA, and BEN are funneled through the CAT branch, and HBA and VAN are funnelled through the PCA branch of the β-ketoadipate pathway in *R. opacus*.

3.6.4. Transporters for lignin model compounds

Transporter expression control may be related to aromatic tolerance mechanisms. The putative shikimate transporter (RS31355), which was significantly upregulated in other phenol-adapted *R. opacus* strains (Yoneda et al., 2016), was also upregulated in PHE (281–299-fold) and the mixture (87–295-fold) for both WT and PVHG6 relative to the glucose condition at both time points (Table S11). An MFS transporter (RS33590) was moderately upregulated in response to PCA precursors VAN (137–193-fold) and HBA (10–15-fold), and the mixture (45–115-fold), but was minimally upregulated by CAT precursors PHE, GUA, and BEN (1.0–3.7-fold) in WT and PVHG6 at both time points (Table S11). Another MFS transporter (RS30810) located adjacent to the BEN degradation cluster was upregulated in BEN (1330–1720-fold) and the mixture (958–2620-fold) for both WT and PVHG6 at the first time point. At the second time point, the MFS transporter was downregulated in PVHG6 compared to the WT strain in a similar manner to the BEN degradation cluster (Fig. 5A). The MFS transporter RS30810 was also moderately upregulated by CAT precursor GUA (57–62-fold), but only minimally upregulated by PCA precursors VAN (1.6–7.5-fold) and HBA (1.1–8.7-fold) in both strains compared to the glucose condition. The branch-dependent upregulation of MFS transporters RS33590 and RS30810 is similar to what was observed for the β-ketoadipate pathway (Fig. 6). Overall, we observed multiple transporters whose expression was responsive to lignin model compounds.

To explore the role of transporters in aromatic tolerance and utilization, we compared the growth of three putative transporter knockout mutants (RS31355, RS33590, and RS30810) to that of the WT strain using different carbon sources (Fig. S18). The growth of these knockout mutants and the WT strain were compared using 0.75 g/L PHE, 1.25 g/L GUA, 1.75 g/L VAN, 2 g/L HBA, 5 g/L BEN, and the combined mixture (2.5 g/L total aromatics) as sole carbon sources. The putative shikimate transporter (RS31355) knockout mutant had lower cell densities (OD_{600}) after 48 h than the WT strain using PHE and the mixture as sole carbon sources, which matches previous reports of RS31355 having a role in PHE transport (Yoneda et al., 2016). The putative vanillate transporter (RS33590) knockout mutant had lower OD_{600} values than the WT strain using VAN, PHE, and the mixture as sole carbon sources. The putative benzoate transporter (RS30810) knockout mutant had lower OD_{600} values than the WT strain using BEN, VAN, GUA, PHE, and the mixture as sole carbon sources (Fig. S18). None of the transporter knockout mutants exhibited growth impairments on HBA (Fig. S18). The impaired growth of the putative aromatic transporter knockout mutants on some compounds suggests transporter specificity and that the influx or efflux of aromatic compounds plays an important role in aromatic tolerance and utilization (Fig. S18).

3.6.5. By-product degradation pathways

The consumption of aromatics can lead to the formation of by-products. We observed upregulation of gene clusters involved in one carbon compound (C1) metabolism during growth on aromatics (Fig. S19). Catabolism of VAN and GUA requires a demethylation step that releases formaldehyde during conversion to PCA and CAT, respectively (Chen et al., 2012; Dardas et al., 1985; Priefert et al., 1997) (Figs. 5, 6). In VAN and GUA growth conditions, we observed the upregulation of a mycothiol-dependent pathway that converts formaldehyde to CO_2, and this pathway is found in *Rhodococcus* strains and other actinomycetes (Lessmeier et al., 2013; Yoshida et al., 2011) (Fig. S19). This pathway (RS31920–RS31930) was upregulated in VAN and GUA (21–105-fold), but expression varied in the mixture from no significant upregulation to 26-fold upregulation for both strains compared to the glucose control. Another pathway for formaldehyde degradation is the ribulose monophosphate (RuMP) pathway, which converts formaldehyde and ribulose-5-phosphate to fructose-6-phosphate for consumption via the pentose phosphate pathway (Orita et al., 2006). The RuMP pathway (RS21455–RS21460) was upregulated in VAN and GUA (450–2600-fold) compared to the glucose condition in both the WT strain and PVHG6. In the mixture, the RuMP pathway was upregulated in the WT strain (23–135-fold) and PVHG6 (3–172-fold) relative to the glucose condition. Genes in the RuMP pathway are also located near the pentose phosphate pathway operon, which was upregulated in a similar pattern to the RuMP pathway (Fig. S19). Together, these results suggest that *R. opacus* has multiple formaldehyde degradation pathways which are activated only when they are necessary (e.g., when VAN or GUA is catabolized, generating the toxic by-product).

3.6.6. Expression of mutated genes identified from comparative genomics

To better understand the effect of mutations on the improved growth phenotype of PVHG6, we compared the expression of genes with mutations found in PVHG6 as well as genes with mutations found in multiple adaptation conditions (Figs. S20, S21). Of the genes with mutations in PVHG6, SOD (RS01890), non-ribosomal peptide synthetase (RS13070), and cytochrome ubiquinol oxidase (RS14825) were highly expressed (> 500 normalized counts) in both the WT and

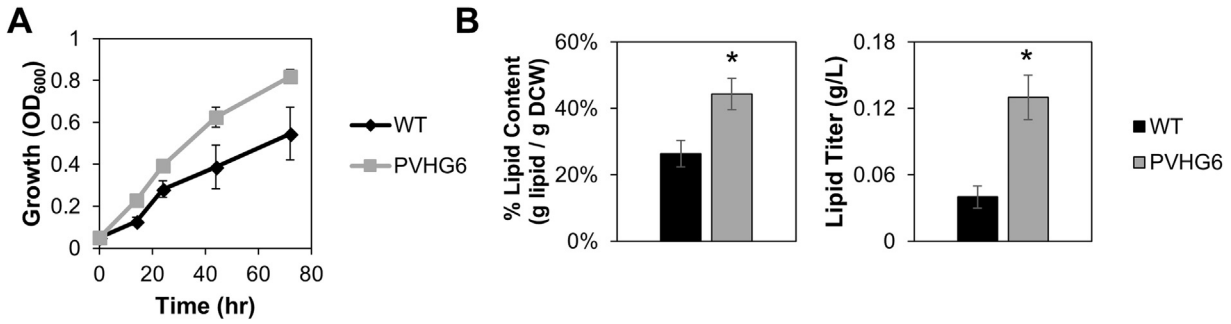

Fig. 7. Conversion of lignin model compounds to lipids. A. Growth of WT and PVHG6 strains in low nitrogen conditions using minimal medium A with 0.5 g/L of PHE, VAN, HBA, GUA, and BEN (2.5 g/L total aromatics) as carbon sources and 0.125 g/L ammonium sulfate as the nitrogen source. B. Lipid content and lipid titer of WT and PVHG6 strains after 72 h of growth in the same growth conditions as A. For all plots, points and bars represent the average of three biological replicates and error bars represent one standard deviation. Asterisk (*) indicates that the difference between WT and PVHG6 values is statistically significant ($P < 0.05$, one mean, two-tailed Student's *t*-test).

PVHG6 strains across all tested growth conditions, including the high glucose condition (Fig. S20, Table S11). For genes with mutations found across multiple adaptation conditions (Fig. 3B, Table S5), SOD (RS01890), cytochrome ubiquinol oxidase (RS14825), phosphoenolpyruvate carboxykinase (RS08140), and fructose bisphosphate aldolase (RS10095) were highly expressed (> 500 normalized counts, Fig. S21, Table S11). These results suggest that mutations could play a role in phenotypic differences between WT and PVHG6 strains, possibly by changing specific enzyme activities (e.g., SOD, Fig. S5), instead of changing expression levels of highly expressed genes (Figs. S20, S21).

3.7. Lipid production using lignin model compounds

To determine the effect of the adaptation on the ability of *R. opacus* to convert lignin model compounds into a bioproduct (e.g., lipids), we compared total lipid production between WT and PVHG6 grown in 2.5 g/L of lignin model compounds (0.5 g/L each of PHE, GUA, HBA, VAN, and BEN) in minimal medium A in a low nitrogen condition (Fig. 7). PVHG6 reached a 50% higher cell density (OD_{600}) than the WT strain after 72 h, and it accumulated 44% of its cell dry weight as lipids, compared to only 26% by WT (Fig. 7). After 72 h, the adapted strain reached a lipid titer of 0.13 g/L using lignin model compounds as a sole carbon source, which is a 225% increase compared to the WT strain (Fig. 7B). These results suggest that adaptive evolution can lead to significant improvements in lipid production by increasing lignin model compound tolerance and consumption.

4. Discussion

Microbial tolerance and consumption of aromatic mixtures is a complex, understudied phenotype that involves numerous interactions between many genes and pathways. An improved understanding of this complex phenotype and its underlying mechanisms is critical for efficient lignin valorization. In this work, we investigated lignin model compound tolerance and utilization by combining adaptive evolution and multi-omic approaches. We demonstrated that *R. opacus* can be adaptively evolved to improve consumption of aromatic mixtures, and we identified shared mutations in adapted strains from multiple adaptation experiments that could affect aromatic tolerance and utilization. We observed that the adapted strain PVHG6 had higher aromatic consumption rates than the WT strain in a mixture of lignin model compounds, and we identified five upregulated funneling pathways and two by-product detoxification pathways that were responsive to specific lignin model compounds. Furthermore, our results demonstrate that enzymatic activities which affect levels of intracellular molecular oxygen and superoxide radicals likely play an important role in aromatic tolerance and utilization. Overall, this work highlights the value of combining adaptive evolution with a multi-omic approach to provide insights into microbial aromatic tolerance and utilization, to create improved strains for aromatic mixture consumption, and to identify novel targets for engineering *R. opacus* strains toward lignin valorization.

The ability of *R. opacus* to successfully adapt to a mixture of lignin model compounds in a relatively small number of generations could be related to its relatively high mutation rate. Across all adaptation experiments, we observed an average of 32 mutations after ~270–420 generations (~4 generations per subculture) (Tables S1, S11), which is at least an order of magnitude higher than rates of occurrence observed in *Escherichia coli* under stress conditions (Lee et al., 2011). Even in the high glucose condition, the average mutation occurrence was 19 mutations after ~290 generations in *R. opacus*. This high occurrence of mutations was not the result of any mutations in the DNA recombination and repair system, which are often found in hypermutator strains (Chu et al., 2017; Sandberg et al., 2014; Sniegowski et al., 1997). Notably, a large portion of SNPs observed in *R. opacus* were synonymous SNPs (Table S2). While synonymous SNPs could potentially affect gene expression rates, protein folding, and thus protein functions (Kimchi-Sarfaty et al., 2007), most synonymous SNPs in both the glucose and aromatic adaptation conditions were located in the same region of Plasmid 1, suggesting that these mutations are not related specifically to aromatic tolerance and utilization.

The most frequently mutated genes in *R. opacus* were related to redox reactions (Fig. 3B). One such example was SOD, a highly conserved enzyme that protects cells from superoxide radicals (O_2^-) by converting them into molecular oxygen (O_2) or hydrogen peroxide (H_2O_2) (Miller, 2012). We also observed multiple mutations affecting cytochrome ubiquinol oxidase in all phenolic compound adapted strains, but not in the high glucose or BEN adapted strains. This gene was also mutated in a previous *R. opacus* adaptation experiment using phenol as a sole carbon source (Yoneda et al., 2016). Cytochrome ubiquinol oxidase catalyzes the terminal step in one of the electron transport chains present in *Rhodococcus* strains, which reduces O_2 to H_2O (Kishikawa et al., 2010). The exact mechanistic contribution of these two mutated enzymes to the evolved aromatic phenotypes is not fully understood, but the known utilization of superoxide radicals and O_2 during aromatic consumption may provide some insights. Superoxide radicals are generated from O_2 by aromatic degradation enzymes, including monooxygenase funneling enzymes (e.g., HBA monooxygenase) (Gatti et al., 1994) and ring splitting dioxygenases (e.g., catechol 1,2-dioxygenase) (Bugg, 2001), to facilitate aromatic catabolism. Our observation that PVHG6 had a 56% decreased SOD activity relative to the WT strain suggests a greater availability of superoxide radicals for aromatic degradation enzymes in PVHG6 than the WT strain.

By performing transcriptomic analyses on strains grown on single compounds, we were able to identify distinct funneling pathways for

five lignin model compounds (Fig. 5) and two aromatic by-product detoxification pathways (Fig. S19). The responses of funneling pathways to individual compounds and the mixture (Fig. 5A), together with a distinct consumption pattern of lignin model compounds in the mixture (Fig. 4B), suggest that *R. opacus* can differentially and specifically regulate aromatic utilization pathways in response to specific compounds. Carbon catabolite repression in *Rhodococcus* strains has been reported between aromatic compounds such as benzoate and phthalate (Choi et al., 2007) and 4-methoxybenzoate and 2-ethoxyphenol (Karlson et al., 1993). Relatedly, we observed differential upregulation of guaiacol degradation cluster #2 between the GUA growth condition and the mixture in both WT and PVHG6 strains (Fig. 5A), suggesting that the presence of other aromatic compounds may delay guaiacol consumption (Fig. 4B) by reducing the expression level of guaiacol degradation cluster #2. Additionally, two pathways for a by-product of VAN and GUA catabolism, formaldehyde, in addition to the gluconeogenesis and pentose phosphate pathway genes that produce required enzymatic substrates, were all upregulated in both strains in the VAN, GUA, and mixture growth conditions (Fig. S19). Several transporter genes were also upregulated, and gene knockout experiments demonstrated their importance for aromatic utilization or tolerance, as suggested previously (Yoneda et al., 2016). Together, these results show that *R. opacus* encodes a complex catabolic network for aromatic utilization, which includes a number of aromatic transporters and metabolic pathways that are regulated in a compound-specific manner.

In our previous report, we performed adaptive evolution using phenol as a sole carbon source (Yoneda et al., 2016). Because lignin depolymerization generates heterogeneous aromatic mixtures, understanding tolerance and utilization mechanisms for a greater diversity of aromatic compounds and mixtures is necessary for lignin valorization. Accordingly, our current work tackles a substantially expanded set of adaptive evolution experiments on multiple lignin model compounds (including phenol) and their mixtures. From this large number of evolved trajectories, we chose six adaptive evolution experiments which represented both substrate diversity and mixture complexity, and performed comparative multi-omic analyses of selected mutant strains that were grown in these diverse aromatic carbon sources. Our comprehensive, multi-omic analyses allowed for elucidation of improved aromatic catabolism in evolved *R. opacus* strains as well as identification of multiple compound-specific pathways, facilitating future lignin valorization efforts.

Acknowledgement

The authors thank members of the Dantas, Moon, and Foston labs for scientific discussions and critical review of the manuscript, and Jessica Hoisington-Lopez, Eric Martin, and Brian Koebbe in the Edison Family Center for Genome Sciences and Systems Biology at the Washington University in St. Louis School of Medicine for Illumina sequencing and high-throughput computing support. This work was supported by the U.S. Department of Energy [Grant nos. DE-SC0012705 and DE-SC0018324 to GD, TSM, and MF].**Conflict of interest**

The authors declare that they have no conflict of interest.

Author contributions

MF, TSM, and GD conceived the project. WRH, TC, DMD, YG, BB, and SJK performed experiments. WRH, TC, DMD, TSM, and GD analyzed the results. WRH, TC, DMD, MF, TSM, and GD wrote the manuscript.

Accession numbers

Genomic and transcriptomic sequences have been deposited with the Sequence Read Archive (SRA) of the National Center for Biotechnology Information (NCBI) under accession number SRP131196.

Appendix A. Supplementary material

Supplementary data associated with this article can be found in the online version at doi:10.1016/j.ymben.2018.06.009.

References

Alvarez, H.M., Mayer, F., Fabritius, D., Steinbuchel, A., 1996. Formation of intracytoplasmic lipid inclusions by *Rhodococcus opacus* strain PD630. Arch. Microbiol. 165, 377–386.
Ashburner, M., Ball, C.A., Blake, J.A., Botstein, D., Butler, H., Cherry, J.M., Davis, A.P., Dolinski, K., Dwight, S.S., Eppig, J.T., et al., 2000. Gene ontology: tool for the unification of biology. The Gene Ontology Consortium. Nat. Genet. 25, 25–29.
Balan, V., Chiaramonti, D., Kumar, S., 2013. Review of US and EU initiatives toward development, demonstration, and commercialization of lignocellulosic biofuels. Biofuels Bioprod. Bioref. 7, 732–759.
Baym, M., Kryazhimskiy, S., Lieberman, T.D., Chung, H., Desai, M.M., Kishony, R., 2015. Inexpensive multiplexed library preparation for megabase-sized genomes. PLoS One 10, e0128036.
Bhat, A.H., Dasan, Y.K., Khan, I., 2015. Extraction of lignin from biomass for biodiesel production. In: Hakeem, Khalid Rehman, Jawaid, Mohammad, Alothman, Othman Y. (Eds.), Agricultural Biomass Based Potential Materials. Springer, Cham, pp. 155–179.
Blazeck, J., Hill, A., Liu, L., Knight, R., Miller, J., Pan, A., Otoupal, P., Alper, H.S., 2014. Harnessing *Yarrowia lipolytica* lipogenesis to create a platform for lipid and biofuel production. Nat. Commun. 5, 3131.
Bolger, A.M., Lohse, M., Usadel, B., 2014. Trimmomatic: a flexible trimmer for Illumina sequence data. Bioinformatics 30, 2114–2120.
Bugg, T.D., 2001. Oxygenases: mechanisms and structural motifs for O_2 activation. Curr. Opin. Chem. Biol. 5, 550–555.
Bugg, T.D.H., Rahmanpour, R., 2015. Enzymatic conversion of lignin into renewable chemicals. Curr. Opin. Chem. Biol. 29, 10–17.
Camacho, C., Coulouris, G., Avagyan, V., Ma, N., Papadopoulos, J., Bealer, K., Madden, T.L., 2009. BLAST+: architecture and applications. BMC Bioinform. 10, 421.
Caruccio, N., 2011. Preparation of next-generation sequencing libraries using Nextera technology: simultaneous DNA fragmentation and adaptor tagging by in vitro transposition. Methods Mol. Biol. 733, 241–255.
Chen, H.P., Chow, M., Liu, C.C., Lau, A., Liu, J., Eltis, L.D., 2012. Vanillin catabolism in *Rhodococcus jostii* RHA1. Appl. Environ. Microbiol. 78, 586–588.
Chen, Y., Ding, Y., Yang, L., Yu, J., Liu, G., Wang, X., Zhang, S., Yu, D., Song, L., Zhang, H., et al., 2014. Integrated omics study delineates the dynamics of lipid droplets in *Rhodococcus opacus* PD630. Nucleic Acids Res. 42, 1052–1064.
Choi, K.Y., Zylstra, G.J., Kim, E., 2007. Benzoate catabolite repression of the phthalate degradation pathway in *Rhodococcus* sp. strain DK17. Appl. Environ. Microbiol. 73, 1370–1374.
Chu, N.D., Clarke, S.A., Timberlake, S., Polz, M.F., Grossman, A.D., Alm, E.J., 2017. A mobile element in mutS drives hypermutation in a marine *Vibrio*. mBio 8, e0204516.
Conrad, T.M., Lewis, N.E., Palsson, B.O., 2011. Microbial laboratory evolution in the era of genome-scale science. Mol. Syst. Biol. 7, 509.
Dardas, A., Gal, D., Barrelle, M., Sauret-Ignazi, G., Sterjiades, R., Pelmont, J., 1985. The demethylation of guaiacol by a new bacterial cytochrome P-450. Arch. Biochem. Biophys. 236, 585–592.
DeLorenzo, D.M., Henson, W.R., Moon, T.S., 2017. Development of chemical and metabolite sensors for Rhodococcus opacus PD630. ACS Synth. Biol. 6, 1973–1978.
DeLorenzo, D.M., Rottinghaus, A.G., Henson, W.R., Moon, T.S., 2018. Molecular toolkit for gene expression control and genome modification in Rhodococcus opacus PD630. ACS Synth. Biol. 7, 727–738.
DePristo, M.A., Banks, E., Poplin, R., Garimella, K.V., Maguire, J.R., Hartl, C., Philippakis, A.A., del Angel, G., Rivas, M.A., Hanna, M., et al., 2011. A framework for variation discovery and genotyping using next-generation DNA sequencing data. Nat. Genet. 43, 491–498.
Dionisio, F., Conceicao, I.C., Marques, A.C., Fernandes, L., Gordo, I., 2005. The evolution of a conjugative plasmid and its ability to increase bacterial fitness. Biol. Lett. 1, 250–252.
Dunlop, M.J., 2011. Engineering microbes for tolerance to next-generation biofuels. Biotechnol. Biofuels 4, 32.
Fischer, C.R., Klein-Marcuschamer, D., Stephanopoulos, G., 2008. Selection and optimization of microbial hosts for biofuels production. Metab. Eng. 10, 295–304.
Folch, J., Lees, M., Sloane Stanley, G.H., 1957. A simple method for the isolation and purification of total lipides from animal tissues. J. Biol. Chem. 226, 497–509.
Gatti, D.L., Palfey, B.A., Lah, M.S., Entsch, B., Massey, V., Ballou, D.P., Ludwig, M.L., 1994. The mobile flavin of 4-OH benzoate hydroxylase. Science 266, 110–114.
Gotz, S., Garcia-Gomez, J.M., Terol, J., Williams, T.D., Nagaraj, S.H., Nueda, M.J., Robles, M., Talon, M., Dopazo, J., Conesa, A., 2008. High-throughput functional annotation and data mining with the Blast2GO suite. Nucleic Acids Res. 36, 3420–3435.
Gröning, J.A.D., Eulberg, D., Tischler, D., Kaschabek, S.R., Schlömann, M., 2014. Gene redundancy of two-component (chloro)phenol hydroxylases in Rhodococcus opacus 1CP. FEMS Microbiol. Lett. 361, 68–75.
Hahn-Hagerdal, B., Galbe, M., Gorwa-Grauslund, M.F., Liden, G., Zacchi, G., 2006. Bio-

ethanol- the fuel of tomorrow from the residues of today. Trends Biotechnol. 24, 549–556.
Harrison, E., Brockhurst, M.A., 2012. Plasmid-mediated horizontal gene transfer is a coevolutionary process. Trends Microbiol. 20, 262–267.
Harwood, C.S., Parales, R.E., 1996. The beta-ketoadipate pathway and the biology of self-identity. Annu. Rev. Microbiol. 50, 553–590.
Henske, J.K., Gilmore, S.P., Knop, D., Cunningham, F.J., Sexton, J.A., Smallwood, C.R., Shutthanandan, V., Evans, J.E., Theodorou, M.K., O'Malley, M.A., 2017. Transcriptomic characterization of *Caecomyces churrovis*: a novel, non-rhizoid-forming lignocellulolytic anaerobic fungus. Biotechnol. Biofuels 10, 305.
Holder, J.W., Ulrich, J.C., DeBono, A.C., Godfrey, P.A., Desjardins, C.A., Zucker, J., Zeng, Q., Leach, A.L., Ghiviriga, I., Dancel, C., et al., 2011. Comparative and functional genomics of *Rhodococcus opacus* PD630 for biofuels development. PLoS Genet. 7, e1002219.
Ibraheem, O., Ndimba, B.K., 2013. Molecular adaptation mechanisms employed by ethanologenic bacteria in response to lignocellulose-derived inhibitory compounds. Int. J. Biol. Sci. 9, 598–612.
Jin, Y.S., Cate, J.H., 2017. Metabolic engineering of yeast for lignocellulosic biofuel production. Curr. Opin. Chem. Biol. 41, 99–106.
Jones, J.A., Vernacchio, V.R., Sinkoe, A.L., Collins, S.M., Ibrahim, M.H.A., Lachance, D.M., Hahn, J., Koffas, M.A.G., 2016. Experimental and computational optimization of an Escherichia coli co-culture for the efficient production of flavonoids. Metab. Eng. 35, 55–63.
Jones, P., Binns, D., Chang, H.Y., Fraser, M., Li, W., McAnulla, C., McWilliam, H., Maslen, J., Mitchell, A., Nuka, G., et al., 2014. InterProScan 5: genome-scale protein function classification. Bioinformatics 30, 1236–1240.
Karlson, U., Dwyer, D.F., Hooper, S.W., Moore, E.R., Timmis, K.N., Eltis, L.D., 1993. Two independently regulated cytochromes P-450 in a *Rhodococcus rhodochrous* strain that degrades 2-ethoxyphenol and 4-methoxybenzoate. J. Bacteriol. 175, 1467–1474.
Keating, D.H., Zhang, Y., Ong, I.M., McIlwain, S., Morales, E.H., Grass, J.A., Tremaine, M., Bothfeld, W., Higbee, A., Ulbrich, A., et al., 2014. Aromatic inhibitors derived from ammonia-pretreated lignocellulose hinder bacterial ethanologenesis by activating regulatory circuits controlling inhibitor efflux and detoxification. Front. Microbiol. 5, 402.
Kelley, L.A., Mezulis, S., Yates, C.M., Wass, M.N., Sternberg, M.J., 2015. The Phyre2 web portal for protein modeling, prediction and analysis. Nat. Protoc. 10, 845–858.
Kimchi-Sarfaty, C., Oh, J.M., Kim, I.W., Sauna, Z.E., Calcagno, A.M., Ambudkar, S.V., Gottesman, M.M., 2007. A "silent" polymorphism in the MDR1 gene changes substrate specificity. Science 315, 525–528.
Kishikawa, J., Kabashima, Y., Kurokawa, T., Sakamoto, J., 2010. The cytochrome bcc-aa_3-type respiratory chain of *Rhodococcus rhodochrous*. J. Biosci. Bioeng. 110, 42–47.
Kosa, M., Ragauskas, A.J., 2012. Bioconversion of lignin model compounds with oleaginous *Rhodococci*. Appl. Microbiol. Biotechnol. 93, 891–900.
Kurosawa, K., Boccazzi, P., de Almeida, N.M., Sinskey, A.J., 2010. High-cell-density batch fermentation of *Rhodococcus opacus* PD630 using a high glucose concentration for triacylglycerol production. J. Biotechnol. 147, 212–218.
Kurosawa, K., Laser, J., Sinskey, A.J., 2015. Tolerance and adaptive evolution of triacylglycerol-producing *Rhodococcus opacus* to lignocellulose-derived inhibitors. Biotechnol. Biofuels 8, 76.
Kurosawa, K., Wewetzer, S.J., Sinskey, A.J., 2013. Engineering xylose metabolism in triacylglycerol-producing *Rhodococcus opacus* for lignocellulosic fuel production. Biotechnol. Biofuels 6, 134.
Langmead, B., Salzberg, S.L., 2012. Fast gapped-read alignment with Bowtie 2. Nat. Methods 9, 357–359.
Le, R.K., Das, P., Mahan, K.M., Anderson, S.A., Wells Jr., T., Yuan, J.S., Ragauskas, A.J., 2017. Utilization of simultaneous saccharification and fermentation residues as feedstock for lipid accumulation in *Rhodococcus opacus*. AMB Express 7, 185.
Lee, D.H., Feist, A.M., Barrett, C.L., Palsson, B.O., 2011. Cumulative number of cell divisions as a meaningful timescale for adaptive laboratory evolution of *Escherichia coli*. PLoS One 6, e26172.
Lee, J.W., Yi, J., Kim, T.Y., Choi, S., Ahn, J.H., Song, H., Lee, M.H., Lee, S.Y., 2016. Homosuccinic acid production by metabolically engineered Mannheimia succiniciproducens. Metab. Eng. 38, 409–417.
Lenski, R.E., Travisano, M., 1994. Dynamics of adaptation and diversification: a 10,000-generation experiment with bacterial populations. Proc. Natl. Acad. Sci. USA 91, 6808–6814.
Lessmeier, L., Hoefener, M., Wendisch, V.F., 2013. Formaldehyde degradation in Corynebacterium glutamicum involves acetaldehyde dehydrogenase and mycothiol-dependent formaldehyde dehydrogenase. Microbiology 159, 2651–2662.
Li, H., Handsaker, B., Wysoker, A., Fennell, T., Ruan, J., Homer, N., Marth, G., Abecasis, G., Durbin, R., 2009. The sequence alignment/map format and SAMtools. Bioinformatics 25, 2078–2079.
Liao, Y., Smyth, G.K., Shi, W., 2014. featureCounts: an efficient general purpose program for assigning sequence reads to genomic features. Bioinformatics 30, 923–930.
Linger, J.G., Vardon, D.R., Guarnieri, M.T., Karp, E.M., Hunsinger, G.B., Franden, M.A., Johnson, C.W., Chupka, G., Strathmann, T.J., Pienkos, P.T., et al., 2014. Lignin valorization through integrated biological funneling and chemical catalysis. Proc. Natl. Acad. Sci. USA 111, 12013–12018.
Love, M.I., Huber, W., Anders, S., 2014. Moderated estimation of fold change and dispersion for RNA-seq data with DESeq2. Genome Biol. 15, 550.
Madsen, R.B., Jensen, M.M., Morup, A.J., Houlberg, K., Christensen, P.S., Klemmer, M., Becker, J., Iversen, B.B., Glasius, M., 2016. Using design of experiments to optimize derivatization with methyl chloroformate for quantitative analysis of the aqueous phase from hydrothermal liquefaction of biomass. Anal. Bioanal. Chem. 408, 2171–2183.
Miller, A.F., 2012. Superoxide dismutases: ancient enzymes and new insights. FEBS Lett. 586, 585–595.
Nurk, S., Bankevich, A., Antipov, D., Gurevich, A.A., Korobeynikov, A., Lapidus, A., Prjibelski, A.D., Pyshkin, A., Sirotkin, A., Sirotkin, Y., et al., 2013. Assembling single-cell genomes and mini-metagenomes from chimeric MDA products. J. Comput. Biol. 20, 714–737.
Orita, I., Sato, T., Yurimoto, H., Kato, N., Atomi, H., Imanaka, T., Sakai, Y., 2006. The ribulose monophosphate pathway substitutes for the missing pentose phosphate pathway in the archaeon *Thermococcus kodakaraensis*. J. Bacteriol. 188, 4698–4704.
Pandey, M.P., Kim, C.S., 2011. Lignin depolymerization and conversion: a review of thermochemical methods. Chem. Eng. Technol. 34, 29–41.
Patrauchan, M.A., Miyazawa, D., LeBlanc, J.C., Aiga, C., Florizone, C., Dosanjh, M., Davies, J., Eltis, L.D., Mohn, W.W., 2012. Proteomic analysis of survival of *Rhodococcus jostii* RHA1 during carbon starvation. Appl. Environ. Microbiol. 78, 6714–6725.
Pereira, B., Li, Z.J., De Mey, M., Lim, C.G., Zhang, H., Hoeltgen, C., Stephanopoulos, G., 2016. Efficient utilization of pentoses for bioproduction of the renewable two-carbon compounds ethylene glycol and glycolate. Metab. Eng. 34, 80–87.
Pham, H.L., Wong, A., Chua, N., Teo, W.S., Yew, W.S., Chang, M.W., 2017. Engineering a riboswitch-based genetic platform for the self-directed evolution of acid-tolerant phenotypes. Nat. Commun. 8, 411.
Pienkos, P.T., Zhang, M., 2009. Role of pretreatment and conditioning processes on toxicity of lignocellulosic biomass hydrolysates. Cellulose 16, 743–762.
Priefert, H., Rabenhorst, J., Steinbuchel, A., 1997. Molecular characterization of genes of *Pseudomonas* sp. strain HR199 involved in bioconversion of vanillin to protocatechuate. J. Bacteriol. 179, 2595–2607.
Qiao, K., Wasylenko, T.M., Zhou, K., Xu, P., Stephanopoulos, G., 2017. Lipid production in Yarrowia lipolytica is maximized by engineering cytosolic redox metabolism. Nat. Biotechnol. 35, 173–177.
Ragauskas, A.J., Beckham, G.T., Biddy, M.J., Chandra, R., Chen, F., Davis, M.F., Davison, B.H., Dixon, R.A., Gilna, P., Keller, M., et al., 2014. Lignin valorization: improving lignin processing in the biorefinery. Science 344, 1246843.
Rodriguez, A., Salvachúa, D., Katahira, R., Black, B.A., Cleveland, N.S., Reed, M., Smith, H., Baidoo, E.E.K., Keasling, J.D., Simmons, B.A., et al., 2017. Base-catalyzed depolymerization of solid lignin-rich streams enables microbial conversion. ACS Sustain. Chem. Eng. 5, 8171–8180.
Sandberg, T.E., Pedersen, M., LaCroix, R.A., Ebrahim, A., Bonde, M., Herrgard, M.J., Palsson, B.O., Sommer, M., Feist, A.M., 2014. Evolution of *Escherichia coli* to 42 °C and subsequent genetic engineering reveals adaptive mechanisms and novel mutations. Mol. Biol. Evol. 31, 2647–2662.
Shuai, L., Amiri, M.T., Questell-Santiago, Y.M., Heroguel, F., Li, Y., Kim, H., Meilan, R., Chapple, C., Ralph, J., Luterbacher, J.S., 2016. Formaldehyde stabilization facilitates lignin monomer production during biomass depolymerization. Science 354, 329–333.
Sniegowski, P.D., Gerrish, P.J., Lenski, R.E., 1997. Evolution of high mutation rates in experimental populations of *E. coli*. Nature 387, 703–705.
Solyanikova, I.P., Emelyanova, E.V., Borzova, O.V., Golovleva, L.A., 2016. Benzoate degradation by Rhodococcus opacus 1CP after dormancy: characterization of dioxygenases involved in the process. J. Environ. Sci. Health Part B Pestic. Food Contam. Agric. Wastes 51, 182–191.
Sun, Y., Cheng, J., 2002. Hydrolysis of lignocellulosic materials for ethanol production: a review. Bioresour. Technol. 83, 1–11.
Tsitko, I.V., Zaitsev, G.M., Lobanok, A.G., Salkinoja-Salonen, M.S., 1999. Effect of aromatic compounds on cellular fatty acid composition of *Rhodococcus opacus*. Appl. Environ. Microbiol. 65, 853–855.
Valdivia, M., Galan, J.L., Laffarga, J., Ramos, J.-L., 2016. Biofuels 2020: biorefineries based on lignocellulosic materials. Microb. Biotechnol. 9, 585–594.
Van den Bosch, S., Renders, T., Kennis, S., Koelewijn, S.F., Van den Bossche, G., Vangeel, T., Deneyer, A., Depuydt, D., Courtin, C.M., Thevelein, J.M., et al., 2017. Integrating lignin valorization and bio-ethanol production: on the role of Ni-Al_2O_3 catalyst pellets during lignin-first fractionation. Green Chem. 19, 3313–3326.
Vardon, D.R., Franden, M.A., Johnson, C.W., Karp, E.M., Guarnieri, M.T., Linger, J.G., Salm, M.J., Strathmann, T.J., Beckham, G.T., 2015. Adipic acid production from lignin. Energy Environ. Sci. 8, 617–628.
Walker, B.J., Abeel, T., Shea, T., Priest, M., Abouelliel, A., Sakthikumar, S., Cuomo, C.A., Zeng, Q., Wortman, J., Young, S.K., et al., 2014. Pilon: an integrated tool for comprehensive microbial variant detection and genome assembly improvement. PLoS One 9, e112963.
Wheeldon, I., Christopher, P., Blanch, H., 2017. Integration of heterogeneous and biochemical catalysis for production of fuels and chemicals from biomass. Curr. Opin. Biotechnol. 45, 127–135.
Xie, S., Sun, Q., Pu, Y., Lin, F., Sun, S., Wang, X., Ragauskas, A.J., Yuan, J.S., 2017. Advanced chemical design for efficient lignin bioconversion. ACS Sustain. Chem. Eng. 5, 2215–2223.
Xu, P., Qiao, K., Ahn, W.S., Stephanopoulos, G., 2016. Engineering Yarrowia lipolytica as a platform for synthesis of drop-in transportation fuels and oleochemicals. Proc. Natl. Acad. Sci. USA 113, 10848–10853.
Yang, J.E., Park, S.J., Kim, W.J., Kim, H.J., Kim, B.J., Lee, H., Shin, J., Lee, S.Y., 2018. One-step fermentative production of aromatic polyesters from glucose by metabolically engineered Escherichia coli strains. Nat. Commun. 9, 79.
Yates, C.M., Filippis, I., Kelley, L.A., Sternberg, M.J., 2014. SuSPect: enhanced prediction of single amino acid variant (SAV) phenotype using network features. J. Mol. Biol. 426, 2692–2701.
Yoneda, A., Henson, W.R., Goldner, N.K., Park, K.J., Forsberg, K.J., Kim, S.J., Pesesky, M.W., Foston, M., Dantas, G., Moon, T.S., 2016. Comparative transcriptomics elucidates adaptive phenol tolerance and utilization in lipid-accumulating *Rhodococcus opacus* PD630. Nucleic Acids Res. 44, 2240–2254.
Yoshida, N., Hayasaki, T., Takagi, H., 2011. Gene expression analysis of methylotrophic

oxidoreductases involved in the oligotrophic growth of *Rhodococcus erythropolis* N9T-4. Biosci. Biotechnol. Biochem. 75, 123–127.
Zhou, Y.J., Buijs, N.A., Zhu, Z., Gomez, D.O., Boonsombuti, A., Siewers, V., Nielsen, J., 2016a. Harnessing yeast peroxisomes for biosynthesis of fatty-acid-derived biofuels and chemicals with relieved side-pathway competition. J. Am. Chem. Soc. 138, 15368–15377.
Zhou, Y.J., Buijs, N.A., Zhu, Z., Qin, J., Siewers, V., Nielsen, J., 2016b. Production of fatty acid-derived oleochemicals and biofuels by synthetic yeast cell factories. Nat. Commun. 7, 11709.